Development of Reaction Injection Moulded Polyurethane Foam Including Assessment of Densification and Reinforcement for use as a Structural Core in Rotationally Moulded Products

A thesis submitted in partial fulfilment

of the requirements for the degree

of

Master of Science (Technology)

at

The University of Waikato

By

Nicholas Gerard Maarhuis

THE UNIVERSITY OF
WAIKATO
Te Whare Wānanga o Waikato

‘Plan your work and work your plan’

This page intentionally

left blank (-ish)

Abstract

To improve the performance of specific rotomoulded products being developed at a local company, reinforcement of the hollow core of the products with reaction injection moulded polyurethane (RIM PU) foam was investigated. Improvement of the foam mechanical properties was also investigated, with density variation and the addition of short glass fibre reinforcement.

Testing showed the foam's mechanical properties were not directly relative to density. When foam density was doubled from 300 to 600kg/m^3, the tensile strength increased by a factor of 2.7 and the modulus by a factor of 2.5. For ME1020 (fibre type) 6mm chopped fibre reinforced foam, these increases were larger, at factors of 3.0 and 2.6 for strength and modulus, respectively. For 300kg/m^3 foam, fibre made negligible difference to the tensile strength, but the ME1020 reinforced foam was found to have 29% higher modulus than the neat foam at the same density (for 5wt% fibre composites). The 101C (fibre type) reinforced foam performed poorly, even showing a decrease in strength when compared to the neat foam at 600kg/m^3 (for 5wt% fibre composites). The bending creep properties of reinforced foam was found to be higher than that of the neat foam in most cases, with ME1020 fibre composite foam performing better than 101C fibre reinforced composites in all cases. 5wt% ME1020 fibre reinforced foam was found to have impact strengths over twice that of neat foams at the same density. Impact strength improvements were also seen for 101C fibre reinforced foam, but to a lesser extent for both foam densities tested.

Morphological analysis of foam tensile fracture surfaces was undertaken and many interesting observations were made. Features such as cell elongation and fibre alignment with the foam flow direction were consistent with foam literature, but some unique features were observed. These include a localised 'string' cell packing trend, and also microscopic areas of localised plastic deformation in cell walls, which were visible as wrinkled surfaces on the foam cell walls.

Modification of the (rotomoulded) skin to foam interface was investigated, as this parameter will likely affect the service performance of the whole product. Experimentation with various methods to increase the skin/foam interfacial shear strength was undertaken, and large improvements were attained with methods trialled and developed. These included adding particles to the rotomoulding charge, which became embedded in the inner skin of the moulded part, and protrude from the inner surface. These particles ‘key’ into the foam which fills the product’s hollow core. Other interfacial shear strength improvement concepts for equipment to be developed were also proposed. One concept proposed is an innovative modification to plasma treatment equipment currently available, which could be used to treat the inner surface of hollow products, to improve the bonding between the inner rotomoulded surface and the foam. Another concept is proposed which may oxidise the inner rotomoulded part surface, but, only at the very end of the rotomoulding cycle, so that the bulk polymer is not degraded. The purpose of this deliberate oxidation is to achieve results similar to those attained by plasma or flame treatment currently used by industry for improving the wettability of PE products.

Acknowledgements

I may never do a PhD or get an Oscar, so this could get emotional…

First and foremost, my gratitude goes to Tina and Gerard, the best parents in the Alicetown-Eastbourne area, for endowing me with your good looks, intelligence, and tenacity to *master* all my endeavours, and thanks also for taking good care of my baby while I was away at university all these years.

Thanks to my fantastic sisters, Anita and Michelle, for always being there for me, and to all my friends, who have helped sculpt me into the person I am today.

Immense thanks go to my affable and transcendent academic supervisor Dr Kim Pickering. The smell of banana cake will forever remind me of your jocoseness and warm personality.

Many thanks go to my industry supervisor Rodney Lawrence. I have learnt invaluable lessons in innovation and business from you which I will take forward with me.

Big thanks go out to Paul Betschart. It's been awesome working alongside you.

Thanks to Sandy and the team at ITS. It has been fantastic working with you.

Thanks to all the other people who have helped me, including Cheryl Ward (you're a lifesaver), the lab technicians: Yuanji, Paul and Brett, the CAKE group, Mary for all your help, Helen Turner for your SEM prowess, Barry O'Brien for the light box imaging, and Dean Aldridge at SGS Hamilton for the X-raying.

Thank you to the Foundation for Research, Science and Technology, for the Technology for Industry Fellowships (TIF) funding.

Thanks to the Baileys and the Laings for their hospitality on my many visits to Tauranga over the last two years, and to the Goldsburys for having me while I wrote my thesis.

I would like to bulk-thank all the teachers and lecturers I've had who have made learning a fun and enjoyable experience for me. I will never forget the wise words of my Hutt Valley High 6th form physics teacher Mr Clitheroe, on the topic of gravity, jokingly proclaiming 'the earth sucks'.

Last but not least, cheers to The Outies, for without which I'm not sure I would've made it through my years in Hamilton. We had some fun didn't we.

Table of Contents

1 Introduction

1.1 Product Requirements

The purpose of this research project was to maximise the product performance of specific rotationally moulded (or 'rotomoulded') export products being developed at a local company. The method of improvement was to fill the hollow core of the product with high density reaction injection moulded (RIM) rigid polyurethane (PU) foam. One aim was to minimise the production and/or material cost while still meeting or (preferably) exceeding the mechanical property requirements of the product. Cost minimisation is important due to the competitive nature of business and the extra freight cost for a New Zealand company exporting around the world. The weight of the product is also a factor, due partly to freighting and partly for the weight in service. Consequently, another aim of the research was to minimise the overall product weight if possible. A low weight fraction of fibre reinforcement is relatively cheap compared to the foam material cost, so short fibre reinforcement of the foam was researched and tested, as there is potential for reinforced foam to have similar or better properties than neat (non-reinforced) foam of higher density.

The rotomoulded products for which this research was commissioned have many important mechanical property requirements, due to their specific and demanding applications. The products will receive large static, cyclic and impact loads, are required to be very rigid, and keep very high dimensional stability for the expected product lifetime of at least 10-15 years. Other specifications include that the products may be exposed to warmer climates (up to or over 40°C), ultraviolet (UV) radiation, and weathering.

1.2 Foam Selection

The foam system selected was ‘Isofoam RM6291W’ reaction injection moulded (RIM) polyurethane (PU). This foam is produced by Baxenden Chemicals Limited and was specified by the company producing the rotomoulded products for which the foam would be used. Baxenden was chosen for the following reasons:

- After trialling a number of other suppliers in NZ, Australia and the UK, Baxenden stood out with regards to professionalism; their products are a very high quality, performed as they specified, and Baxenden have shown themselves to be very reliable and technically capable. They also supply polymers to the competitive and technically demanding European automotive industry,
- Baxenden had previous experience with glass fibre reinforcement of their foams, and they were the only supplier with rigid PU foam with such a wide density range, allowing research and development of a material with a wide range of properties, depending on how it is prepared.

Chapter 2: Literature Review

2.1 Literature Review Overview

This chapter begins with a review of rotational moulding, as this is the manufacturing method of the products for which the foam being researched is to be used. This follows with an investigation into polymer matrix composites (PMCs), including theory on modelling composites, in particular, randomly distributed short fibre composites (because this form of foam reinforcement was to be experimentally tested).

Glass fibre was investigated because previous to this research project, test production of RIM PU foam with various fibre type and length reinforcements were trialled, and 6mm glass fibre was chosen as the most suitable fibre and length for this application. Cost, availability of suitably sized (coated) fibres, and ease of processing were the main factors for the decision to use glass fibre over other options, and 6mm was chosen as the length because longer fibre was problematic to process.

As the main focus of this research project is on a type of polymer foam, the characteristics of polymer foams were investigated. A rotomoulded product filled with foam can be considered as a structure analogous to a composite sandwich structure, if the rotomoulded skin and foam filling are considered to be the sandwich skins and core material, respectively. Sandwich structures were therefore investigated to examine the important mechanical parameters of the foam. The lack of adhesion between PE parts and PU foam is widely known by rotomoulders using these materials [1], so PE surface treatments to improve adhesion were investigated. If the sandwich structure analogy is correct, the skin/foam interfacial strength will likely affect the overall product properties. Wettability is known as an essential precursor to bonding, so a summary of techniques to analyse the wettability of a polymer surface is given.

Environmental issues are pertinent in both academic material research and in industry, both locally and internationally. Legislative, moral and economic considerations will often affect the processes undertaken and/or the outcome of the work. Issues discussed include the economics of being environmentally aware, recycling of PU, ozone depletion from chemical blowing agents in some foams, and other environmental developments which are occurring in industry.

2.2 Rotational Moulding

Rotational moulding (also commonly known as 'rotomoulding', and occasionally 'rotocasting' [2]) is a form of manufacturing whereby thermoplastic polymer powder is placed in a mould and then heated and rotated until the powder sinters and forms a layer of material (or 'skin') on the mould surface. Thermosetting plastics can also be used for rotomoulding, but this is less common. After heating and sintering, when the polymer is fully dense, the mould is cooled down (while still rotating). Finally, the mould is opened for the part to be removed for post-moulding operations such as trimming and drilling. The rotomoulding process is shown schematically in Figure 2.3. It has been used for polymers (initially doll heads made from polyvinylchloride) since the 1940's [3], but a similar technique has been used to make chocolate Easter eggs as early as the 17th century [4]. The wall thickness of the part is determined by the amount of polymer placed in the mould (the 'charge') relative to the mould surface area. If desired, the wall thickness over the length or width of the part can be altered with special control of the longitudinal and/or transverse rotation rates. Rotomoulding cycle times are much longer than most other polymer processing techniques, but the process has the unique ability to produce products which can be hollow, incredibly large, and involve complex surfaces; this is one of the reasons rotomoulding is commonly used to make large liquid storage tanks, up to and over 10,000 litres in volume [4], such as the water tank shown in Figures 2.1 and 2.2. The products made by the rotomoulding industry are shown in Figure 2.4.

Figure 2.1: 10,000 litre water tank [5]

Figure 2.2: Base of water tank in Figure 1.1 [5]

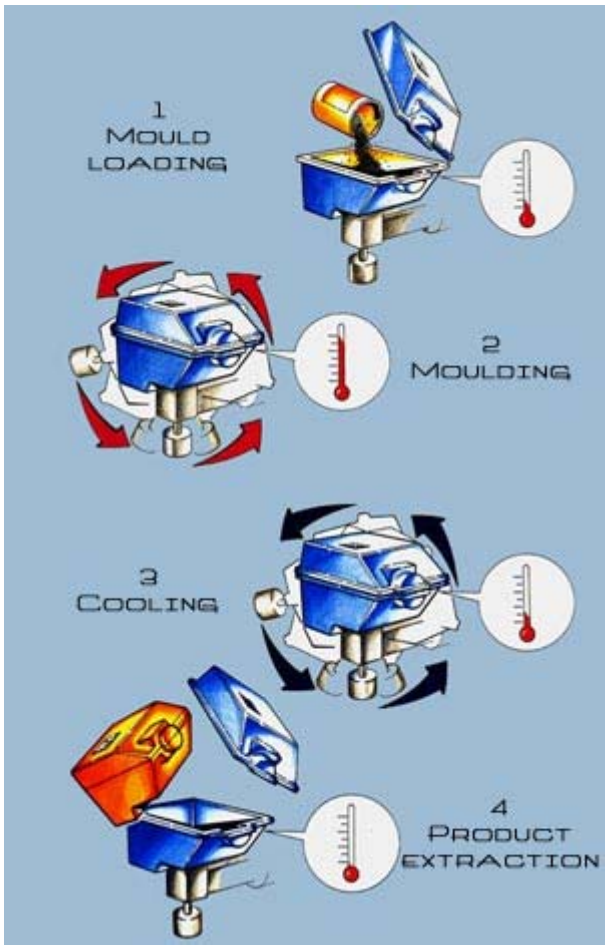

Figure 2.3: The four stages of a rotomoulding cycle [6]

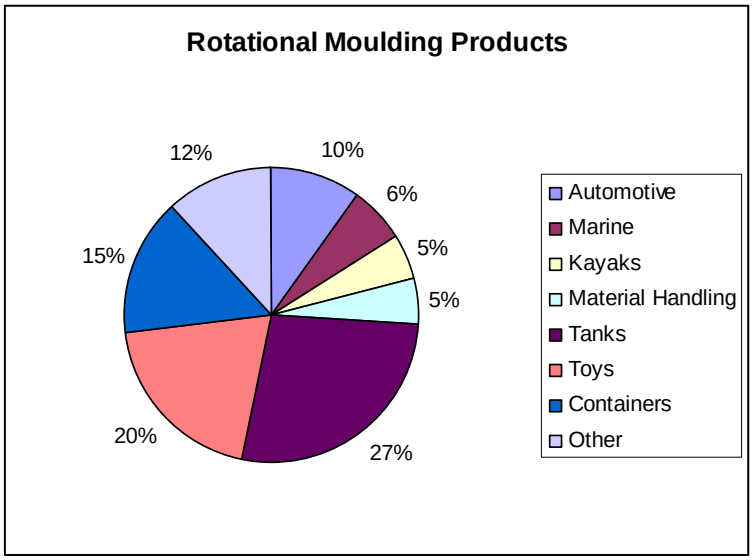

Figure 2.4: Proportion of rotomoulded products per industry [7]

Some examples of the products made using rotomoulding include kayaks (Figure 2.5), vehicle panels, or whole car bodies in the case of the three wheeled electric car shown in Figure 2.6. Recent diversification by rotomoulding manufacturers has lead to the production of designer furniture, with an example being the bathtub shown in Figure 2.8. It is made from opaque white polyethylene (PE) and illuminated with variable multi-colour internal lighting. Matching sinks and lamps are also available. Another product made using rotomoulding is radio frequency identification (RFID) panels for use on farms (shown in Figure 2.7), which have a rotomoulded outer skin and are filled with low density foam for increased strength.

High quality colour graphics can be moulded into rotomoulded products, as well as metal or polymer inserts. Given that all the powder placed in the mould ends up in the moulded product, the only waste material is that which is trimmed/cut/drilled. Waste material can be sent for recycling, as thermoplastics are easily reprocessed. Design features that are used for rotomoulding include ribbing and ‘kiss-offs’ (conical shaped features on both sides of a component, which cause material to flow together and join in the centre, adding stiffness and strength to the product).

Figure 2.5: Rotomoulded kayak [8]

Figure 2.6: Electric car [9]

Figure 2.7: RFID panel [10]

Figure 2.8: Internally illuminated bathtub [11]

2.2.1 Rotomoulding Equipment

There are various types of rotomoulding machines, but they all provide the requisite heating and cooling while rotating the mould/s in two axes. The rotations are slow and not a centrifugal process; typically moulds will rotate between four and twenty times per minute [4]. Most modern rotomoulding machines have full biaxial rotation about two perpendicular axes. Carousel machines are one of the most common types of rotomoulding equipment used today, with most having three or four arms, so that each arm is at a different stage (charging, heating, cooling, and de-moulding), to aid production process efficiency. When full biaxial rotation is not possible (such as for very large moulds) other methods can be used. One is the 'rock and roll' method, which involves the mould rotating 360 degrees about one axis, and rocking backwards and forwards about the second axis.

Moulds are heated in large ovens, or directly by open flames, microwaves, induction heating, infrared heating, or by conduction heating with a liquid such as hot oil. Accurate control of processing time and mould/oven temperatures is required to achieve optimum material processing, resulting in the best material properties; too long at high temperatures or over-heating will degrade the polymer, but too short a processing time or insufficient temperature and the polymer will not fully sinter and densify. Surface pin-holes and voids are signs of un-optimally processed parts.

2.2.2 Rotomoulding Materials

Over ninety percent of the world's rotomoulded products are made from polyethylene (PE) [4], but other thermoplastic powders such as polyvinylchloride (PVC) and polypropylene (PP) are also used for rotomoulding.

Polymers are created by the polymerization of monomers; for example, PE is made by subjecting ethylene gas (C_2H_4) to appropriate temperature and pressure conditions in the presence of suitable catalyst species. The resultant polymer

molecules are long chains of repeating units, as shown below in Figure 0.9, for PE, PP, and PVC.

- Polyethylene (PE): $-CH_2-$
- Polypropylene (PP): $-CH_2-CH(CH_3)-$
- Polyvinylchloride (PVC): $-CH_2-CH(Cl)-$

Figure 0.9: Repeating units in PE, PP, and PVC [12]

Polymers other than PE, PVC and PP, however, account for less than 1% of the plastics used. Typical powder sizes for rotomoulding grade PE are 100-500 micrometres, with most being around 300 micrometres [4]. When heated, thermoplastics soften then become liquid, but return to their solid state when cooled again.

PE is from the polyolefin family of thermoplastics, which derive from the ethylene family of simple olefins [13]. There are many types and grades of PE, which are categorised by density or molecular weight, but the most commonly used rotomoulding PE grades are either low density polyethylene (LDPE) or high density polyethylene (HDPE). LDPE has a lower crystallinity, lower melting point, and lower modulus than HDPE [14]. Typical properties of these two materials are shown in the table (Figure 0.10) below.

Material	Tensile Yield Strength	Tensile Modulus	Impact (Izod, notched)	Cost $US/kg
LDPE	8.3-32.1MPa	0.17-0.7GPa	>0.5J/cm	0.90
HDPE	22.1-31.4MPa	1.08-1.1GPa	0.2-2.1J/cm	0.86

Figure 0.10: Properties of LDPE and HDPE [14]

2.2.3 Comparison with Other Methods

Rotomoulding has the advantage of producing components free of residual stress. Reduction of product part-count is often enabled when changing to rotomoulding from other manufacturing methods such as injection moulding (or from fabrication from other materials such as wood or steel). Part-count reduction can save manufacturing time, labour and/or provide beneficial product features. An example of this is one-piece rotomoulded boat hulls, which unlike laminated fibreglass or fabricated aluminium hulls, have no joints.

Blow moulding is another processing method which produces hollow items. Products made by blow moulding require thicker surfaces to allow for the thickness reduction which occurs when the polymer forms into corners. Rotomoulding, however, results in parts with the corners thicker than the surfaces, so is more suited to structural items than blow moulding. Furthermore, products with complex geometries are difficult to produce using blow moulding.

Injection moulding is the most widely used polymer processing method, due to the rapid cycle times and part quality possible from the manufacturing method. However, due to the high pressures used, parts require much stronger (and more expensive) moulds than rotomoulding, and products have post-moulding residual stress. It is also not possible to make hollow parts or undercuts features.

There are some disadvantages to rotomoulding. The material choice is more limited than other methods, and material costs are higher than equivalent grades for injection moulding due to the special additives required to prevent oxidation during processing, and the cost involved in grinding the polymer to a fine powder. In addition it is difficult to produce fibre-reinforced products [15-17], so the potential mechanical properties of rotomoulding materials are lower than that of fibre-reinforced matrices made by other methods.

2.3 Polymer Matrix Composites

Composite materials are widely used in engineering applications where conventional materials cannot meet the specific strength or stiffness requirements. A composite is defined as a multiphase material that exhibits a significant proportion of the properties of both constituent phases, such that a better combination of properties is realised [12]. Polymer-matrix composites (PMCs) have fibres or particles as the reinforcement (or 'dispersed phase'). When the dispersed phase provides no mechanical benefits, they are considered fillers. Fillers are often purely used to decrease material costs, by replacing some of the polymer volume with the less expensive material. Fibrous reinforcement is used when high mechanical performance is required. The mechanical properties of a composite are dependent upon many factors, but rely largely on the matrix and reinforcement properties and the fractions of each of these phases. The reinforcement orientation/s will affect the isotropy, and the matrix/reinforcement interfacial strength will also affect the mechanical properties, as will voids and impurities present in the material. The fibre length is important with PMCs, as the composite relies upon effective load transmittance from the matrix to the fibre. Below a certain critical fibre length the matrix will deform around the fibre and there will be virtually no load transference. In this situation the fibres are essentially fillers. Typical PMC critical fibre length is approximately 1mm, but will vary for different fibre/matrix combinations [12]. Critical fibre length is determined experimentally or can be calculated if the fibre diameter and fibre/matrix interfacial shear strength are known. Longer fibres transfer more load, increasing the composite mechanical properties. This is why continuous, aligned fibre composites are preferred. However, the shape and size of a PMC product and/or certain manufacturing methods (such as injection moulding) create limitations on the maximum processable fibre length (and the ability to control fibre orientation). Continuous fibre composites usually involve more expensive manufacturing processes such as hand lay-up or filament winding. The processing equipment available will also affect the selection of reinforcement. Although the stiffness of (aligned) short fibre composites can be similar to continuous fibre composites, the strength will be much lower, even at very high fibre aspect ratios (>10,000) and the same volume fraction of fibre [18].

Polymer properties such as strength and stiffness are known to be highly temperature dependent. These and other properties including the creep behaviour of polymers depend on various mechanisms which occur as the temperature is increased toward the glass transition temperature. This includes the breaking of secondary bonds, allowing molecules to slip past each other, which decreases the modulus [19]. It has been observed in polymers with up to 40% short-fibre (randomly oriented) reinforced polymers that they retain the creep properties of the matrix polymer, except the creep modulus at a given strain level is proportionately higher and the strain to failure will diminish [18]. The properties of the fibre/matrix interface in glass-fibre-reinforced composites can play a dominant role in governing not only creep performance, but overall composite performance as well [20]. A study of fibre reinforced composite creep properties by Abdel-Magid et al [21] concluded that the creep behaviour is highly influenced by the shear properties of the matrix, and also the suitability of the fibre sizing to the matrix. The high temperature performance of the matrix is very important; they found at 50°C glass fibre reinforced polyurethane exhibited tertiary creep leading to rupture within a few hours when subjected to about 60% of its flexural strength, while glass fibre reinforced epoxy endured months of loading at 60% of its flexural strength before rupture. The samples were reinforced with continuous fibres (PU – 58%V_f glass, epoxy – 52%V_f glass) and tested along the fibre directions in three-point flexure mode.

2.3.1 Predicting Composite Performance

Comparing theoretical estimates (models) of composite performance with actual test results is a useful tool for composite assessment. Deviations from expected properties can highlight potential problems within the composite, and validified results will allow more accurate prediction of composites prepared in the future.

The well known rule of mixtures (ROM) by Kelly and Tyson [22] is a model proposed for predicting composite strength of aligned, continuous fibre reinforced composites loaded parallel to the fibre orientation. It is shown in equation 1,

below, and a schematic of the model is shown in Figure 2.11 (where σ_c is the strength of the composite, σ_f is the fibre strength, V_f is the volume fraction of the fibre, and σ_m is the matrix strength, and V_m is the volume fraction of the matrix).

$$\sigma_c = V_f \sigma_f + V_m \sigma_m \qquad \text{(equation 1)}$$

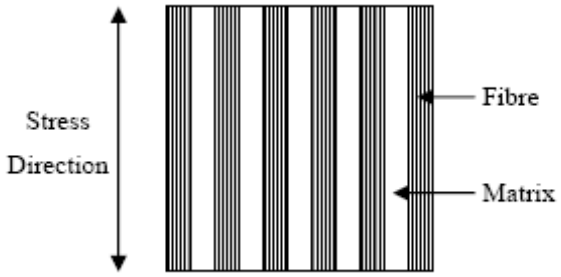

Figure 0.11: Schematic of ROM model [23]

Kelly and Tyson [22] further developed their ROM equation to account for short fibre composites such as this by including a fibre length factor, K_2. For composites with fibres longer than or equal to the critical fibre length, the formula for K_2 is as below (equation 2) (where L_c is the critical fibre length and L is the actual fibre length).

$$K_2 = 1 - L_c/2L \qquad \text{(equation 2)}$$

K_2 for fibres with critical or greater length is derived from the area under the curve in Figure 2.12, divided by the fibre length. Fu and Lauke [24] reported that the tensile strength of short fibre composites approaches a plateau level as the mean fibre length increases for longer (over ~3mm) mean fibre lengths. They also found that the fibre length factor decreased with increasing critical fibre length, which concurs with the Kelly and Tyson [22] formula for K_2.

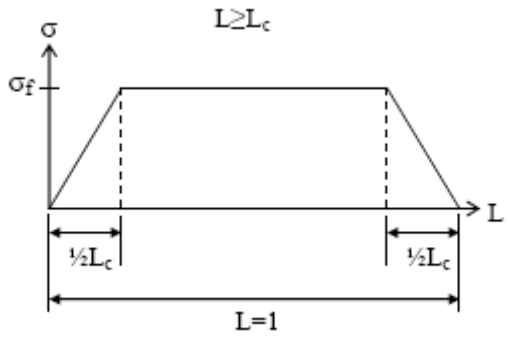

Figure 0.12: Fibre stress distribution schematic [23]

Bowyer and Bader [25] proposed a fibre orientation distribution (FOD) factor, K_1, which was empirically fitted to the Kelly-Tyson ROM equation (creating the 'modified rule of mixtures' [MROM] equation), shown below (equation 3). For randomly oriented fibres a K_1 value of 0.2 has been shown to give good agreement between theoretical and experimental results [26, 27]. An expanded version of the MROM, for randomly oriented short fibres which are equal to or longer than the critical length is shown in equation 4.

$$\sigma_c = K_1 K_2 V_f \sigma_f + V_m \sigma_m \qquad \text{(equation 3)}$$

$$\sigma_c = 0.2 \times (1 - L_c/2L) V_f \sigma_f + V_m \sigma_m \qquad \text{(equation 4)}$$

2.4 Glass Fibre

Glass fibres, although lower strength and stiffness than carbon or aramid fibres (as shown in Figure 2.13, below), are much cheaper and therefore dominate the polymer reinforcement market [28, 29]. The worldwide market for glass fibre in 1997 was 1.5 billion kg, and 95% was E-type glass fibre [30].

Fibre Type	Specific Gravity	Tensile Strength (GPa)	Modulus of Elasticity (GPa)
Aramid (Kevlar)	1.44	3.6-4.1	131
Carbon	1.78-2.15	Up to 4.8	228-724
E-glass	2.58	3.45	72.5

Figure 0.13: Properties of various fibres [12]

As mentioned in Section 0, the fibre/matrix interface is very important to PMC performance. The interfacial strength is highly dependent on the sizing, or 'size' (special coating) applied to fibres when they are produced [20]. Sizings provide a variety of attributes, such as lubricity and strand integrity to enable high speed processing, and compatibility with specific matrix resins to promote strength, stiffness, and durability in the final composite. Glass fibre generally has a sizing layer of 0.2-2% by weight [20].

2.5 Polymer Foams

Polymer foams are also known as cellular, expanded, or sponge polymers. They generally consist of a solid polymer phase and a gaseous phase derived from a blowing agent. There can be more than one polymer and/or fillers/fibres also. Depending on their chemical composition, degree of crystallinity, and degree of cross-linking, they can be categorised as flexible, semi-rigid, or rigid. The cells (or air/gas pockets) can be open (interlinking) or closed. Open-celled foams tend to be flexible, whereas closed-celled foams tend to be rigid. Some polymers can be used to produce foams in densities as low as 1.6kg/m^3, or polymer foams may be up to near the density of the solid material [28, 31]. Foam density is often expressed as a 'relative density'; this is the density of the foam (ρ^*) as a fraction of the solid polymer density (ρ_s), or ρ^*/ρ_s. Mechanical performance is generally proportional to the relative foam density, but can be improved with fibre or particulate reinforcements, so load-bearing rigid foam often has high density and/or fibre reinforcement [28]. Polymer foams are used in applications such as energy absorbing structures, acoustic and thermal insulation, filtering, packaging, and sandwich structures [32].

There are many methods of producing polymer foams, but all of these methods generate gas bubbles in the polymer in its liquid state, which become entrapped when the polymer either cures or cools (and hardens). Methods of bubble creation include use of a chemical blowing agent (CBA), a thermally decomposing blowing agent, mechanical whipping (frothing), expansion of dissolved gas (by

releasing pressure applied to a system), incorporation of hollow microspheres (producing a 'syntactic foam'), and expansion of gas-filled beads with application of heat.

When foams are under compressive loading, cell ribs and/or walls bend and crumple at a critical stress. In low density foams the weakest layer ribs fail first, followed by the other layers, with little or no increase in the stress-strain curve. The transverse dimensions of low density foam specimens change very little even with large compressive strains (up to 50%) [28]. Higher density foams behave more like the non-cellular polymer; after critical stress is reached, the sample will increase in the transverse direction (in a barrel shape), while the foam cells continue to crumple [28].

The structural response of polymer foams strongly depends on the solid material properties, the foam density, and cell morphology such as cell size and shape [31]. Due to the viscoelastic nature of the solid polymer, foams often exhibit strain-rate dependent behaviour [33], although Saha et al [34] concluded that for medium density PU foams (240 and 320 kg/m^3), the strain rate had very minimal effect on peak stress and energy absorption, even over a massive strain rate variation, from quasi-static up to about 1300s^{-1}.

Gibson and Ashby [31] have examined foam extensively and developed models for predicting the performance of various foams with relative density below 0.3. Foam with relative density above 0.3 behaves more similarly to solid polymer [28, 31]. The '2+1 phase model' by Christensen and Lo [35] was used by Saint-Michel et al [32] for modelling PU foams in the relative density range 0.3-0.8, and was found to give more accurate modelling of the foam properties in the linear domain (viscoelastic region) of the stress-strain curve than results obtained using the Gibson and Ashby models.

2.5.1 Foam Morphology

As mentioned in Section 0, foams have open cells and/or closed cells. Closed cells can be roughly or fully spherical in shape or made up of three-dimensional polyhedral cells (such as a combination of rhombic dodecahedrons, pentagonal dodecahedrons, tetrakaidecahedrons, icosahedrons, and others [31]). For example, polyurethane foam has a closed and spherical cellular structure, whereas polyvinylchloride (PVC) foam has a three-dimensional polyhedral structure [32, 33]. Some types of foam have microcells, in which the matrix polymer containing cells is cellular itself [28].

Foam cells can become elongated in the direction of the foaming. The amount of cell elongation can vastly affect the properties and create anisotropy. By increasing the ratio of height to width of a cell (h/d) from 3/5 to 5/3 (by a factor of 2.8), the compressive strength of polyurethane foams may also increase up to 2.8-fold, the tensile strength up to 3-fold, and the shear, bending, and Young's moduli up to 2-fold [36]. Kabir et al found the foam rise direction also effects fracture toughness; when impact test specimens had notches machined parallel to the rise direction, an increase in fracture toughness of up to 27% was observed relative to specimens notched perpendicular to the rise direction [33]. Cell elongation is less pronounced in high density foam produced in closed moulds compared to free rise foam systems, although some elongation occurs near the mould walls for closed mould systems [36].

2.5.2 Rotomoulded Foam

It is possible to process foams using rotomoulding, either with single, double, or triple charges of the mould. For single charge systems, a chemical blowing agent (CBA) is included with the polymer charge, which decomposes towards the end of the heating cycle (once a layer of material has formed onto the mould wall). This foams a portion of the polymer in the mould. For double charge systems, extra polymer and a blowing agent are added once an outer skin has formed, and when the mould returns to heating and rotating, the second charge melts and

foams. Triple charge systems are similar to double charge, but the third charge is plain polymer, so a skin/foam/skin sandwich structure is formed in the wall of the part [37]**.** An example of a double charge system is the 'Rotofoam©' process (developed by Bush and Ademosu [38]) which fill the hollow cavity of rotomoulded products with a low density polystyrene (PS) foam.

Benefits of rotomoulded foam include good skin/foam interfacial strength (when the same polymer is used for the skin and the foam) and the foaming process can be incorporated into the rotomoulding cycle; this negates extra processing steps other systems would require (such as RIM PU injection, which requires product restraining, to prevent expansion due to the expanding foam forces).

The disadvantages of rotomoulded foam are the difficulty to achieve a completely filled part (due to trapped air/gas inside the product) and multi-charge systems require the mould to be removed from the oven during processing, which adds to the manufacturing and oven power costs [39]. There can also be moulding complexities resulting from increased mould pressures due to the gas evolution during the foaming process.

2.5.3 Polyurethane Foam

PU itself was invented by Prof. Dr. Otto Bayer (1902-1982) et.al in 1937 and was initially used as a replacement for rubber. It is now used in products ranging from common items like shoe soles and seat cushioning to technical products such as chemical-resistant coatings and specialty adhesives. PU is available for pouring, spraying, spreading, injecting, extruding, laminating, pultruding, rotomoulding, or casting [40]. It can be made as a foam, in either rigid (for insulation, buoyancy, or structural applications) or flexible forms (for carpet underlay, seat and bed cushioning) [41]. Typical solid (as opposed to foamed) rigid thermosetting PU has a density of 1200kg/m^3, Young's modulus (E) of 1.6 GPa, yield strength of 127 MPa, fracture strength of 130 MPa and fracture toughness (K_{IC}) of 0.35 MPa$\sqrt{m}$ [33]. PU is created by the exothermic reaction of a polyol and a diisocyanate or

polymeric isocyanate in the presence of suitable catalysts and additives, as shown in the below chemical equation (Figure 2.14). The degree of functionality of the polyol and the polyisocyanate determines the degree of cross-linking in the PU [28, 41].

$$xOCN\text{-}R_1\text{-}NCO + xHO\text{-}R_2\text{-}OH \rightarrow -[CONH\text{-}R_1\text{-}NH\text{-}CO\text{-}O\text{-}R_2\text{-}O]\text{-}_x$$

Figure 0.14: Polyurethane chemistry

Water is used as the blowing agent for PU foam; it reacts with isocyanate to form carbon dioxide and urea, as shown in Figure 2.15, below. The expanding gas is trapped during polymerization, creating the foam.

$$2R\text{-}NCO + H_2O \text{ react to give } R\text{-}NH\text{-}CO\text{-}NH\text{-}R + CO_2$$

Figure 0.15: Foaming reaction

With increasing PU foam density, the flexural modulus, flexural strength, and fatigue strength increase [42], as well as the tensile modulus, ultimate stress and strain to failure, and the strain rate sensitivity of failure strength is higher. The fracture toughness is also found to be strongly dependent on the foam density and the microstructure [33, 43].

Reaction injection moulding (RIM) involves mixing monomer and initiator reactive solutions just prior to the injection. This is achieved with high pressure impingement mixing equipment, or mechanical mixing of the two components. Reinforced RIM (RRIM) refers to RIM PU with short glass fibre or glass flake reinforcement. Structural RIM (SRIM) refers to RIM PU reinforced with a preformed (or sprayed) glass fibre mat or fabric. RRIM and SRIM are inaccurate by definition however, as neither are true injection processes. They are open-mould spray processes, but keep the ‘injection’ in the name due to the use of RIM material as the polymer matrix.

2.5.4 Particulate Reinforced Foam

Many trends toward foam developments and reinforcements follow those developed for solid polymer materials, such as the addition of fillers and fibres. Popular fillers include organic and inorganic powders, whiskers, (solid and hollow) microspheres (glass or polymer), and nano-particles. Their purpose is to decrease material cost and sometimes also decrease the density of the foam, however, some fillers have been found to increase the mechanical properties substantially, even when only small volume fractions added [44]. Reinforced foams have finer cells, and are generally more thermally stable than non-reinforced foams [45]. Thorough testing must be done with fillers, as not all filler and foam combinations create better properties [46]; testing of PU foam with calcium carbonate fillers (1-30microns) by Saint-Michel et.al [44] concluded particulate reinforcement of the foam was not efficient if the size of filler added was bigger than the gas pore size of the foam. Alperstein et al [47] found that high modulus particulate fillers can significantly enhance the compressive creep resistance of PU foams, especially at high reinforcement contents and high foam densities.

Low density (88kg/m^3) PU foams have also been made with nano-particle fillers. By dispersing 1-3% by weight of TiO_2 or SiC particles (particle size ~30nm), H.Mahfuz et al [45] were able to achieve approximately 50-70% increases in flexural strength and stiffness over neat foams. It was concluded that the gain in strength was from the delay in the formation and coalescence of initial cracks during loading, due to the nano-particles embedded in the cell walls. However, with higher fractions of particles, both thermal and mechanical properties began to degrade.

2.5.5 Fibre Reinforced Foam

As mentioned in Section 2.4, glass fibre dominates the PMC market, and consequently, similar trends are observed in the composite polymer foam market.

Fibre in composite foam tends to align with foam rise flow direction [48], creating highly anisotropic properties. Studies of chopped-fibre reinforced PU foam by Cotgreave and Shortall [49] found that the presence of fibres gave rise to localised change in morphology of the foam, and increased the tensile properties. Fibre surface treatment and bundle size were also found to affect the morphology. Alonso et al [48] found that fibres can greatly increase the tensile and flexural properties, but usually have a smaller effect on compressive properties; this was also found by Huang et al [50]**.** The fibre type can also affect a composite's anisotropy, foam cell morphology, and therefore, the mechanical properties. Shen and Nutt [51] found that glass fibres aligned with the foam direction better than Nomex fibres. For 10% glass fibre reinforced 80kg/m^3 phenolic foams, samples had double the modulus and 31% higher strength than neat foam, when compression tested parallel to the foam rise direction. Smaller increases were found when the samples were tested perpendicular to the foam rise direction. Alanso et al [48] observed cell sizes for 2.5% aramid fibre reinforced foams were half the size of cell sizes for 2.5% glass fibre reinforced epoxy foams. The finer cell sizes were found to correspond with enhanced compression strength and modulus.

During processing of short fibre composite foams, the fibre length distribution (FLD) and fibre orientation distribution (FOB) evolve, so the final FLD and FOB are impossible to accurately deduce from the original composition information or by simple estimation [52]. A widely used method of examining these effects is by parallel dissection and image analysis of polished surfaces, although Shen et.al [52] recently used high resolution computerised tomography (micro-CT) imaging to attain more detailed information (using a Skyscan 1072 and also VGStudio and Auto-CAD computer programs for analysis). It was found that for 80kg/m^3

phenolic foam with 5wt% short glass fibre (6.4mm), a large amount of fibre breakage occurred, and that the fibres tended to align with the foam rise direction.

Alonso et al [48] found the shear properties and fracture resistance of reinforced epoxy foams are often higher than their neat counterparts; shear strength doubled when 2.5% short glass fibre (6.3mm) was added to the foam. Increasing the glass fibre loading to 5% resulted in shear strength only 1.3 times that of the un-reinforced foam however, which shows composite foam properties are not proportional to the reinforcement loading as may be expected. The importance of fibre sizing was also shown, with correctly sized fibre-reinforced foams exhibiting a two-fold improvement in compressive modulus and a five-fold increase in compressive strength compared with similar composite foams reinforced with untreated glass fibres.

Glass fibre reinforced polymer foams (GFRPF) are a relatively new area of material science, and as such, much development of theoretical models has yet to occur. Shen and Nutt [51] commented that a mechanistic model capable of predicting the behaviour and properties of composite foam is needed, which would incorporate basic parameters such as fibre strength/stiffness, fibre length, fibre loading, orientations, and foam density.

2.6 Sandwich Structures

A sandwich structure is defined by The American Society for Testing Materials (ASTM) as a laminar construction comprising a combination of alternating dissimilar simple or composite materials assembled and intimately fixed in relation to each other so as to use the properties of each to attain specific structural advantages for the whole assembly [53]. Sandwich structures are used as structural members in boats, ships, aeroplanes, and many other load bearing, weight critical situations. They are also used for low/non load bearing walls, doors, or panels for thermal or sound insulation [54]. Sandwich panels act similarly to an I-beam, with high strength faces carrying the compressive and tensile loads, but instead of a thin vertical (high strength) central member, a lightweight core carries

the shear forces (when loaded in bending), as shown in Figure 0.16; the shear properties of a core material are therefore one of the most critical factors, but the compressive modulus and strength are also important [48]. By increasing the core thickness, and therefore the structure's second moment of area (or 'I' value), increases in bending strength and stiffness can be attained with relatively small increases in weight and cost.

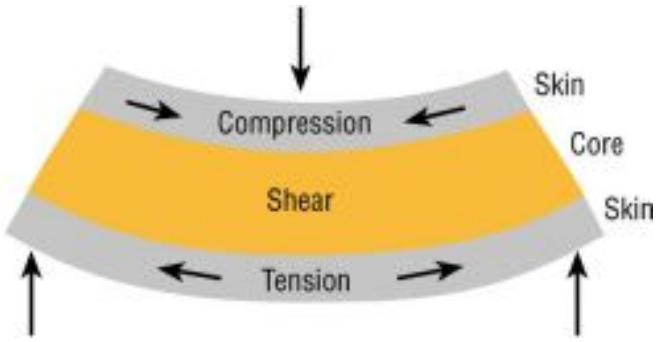

Figure 0.16: Sandwich structure bending schematic [54]

Often the faces will be an aluminium sheet or a fibre reinforced polymer, and the core a paper or aluminium honeycomb, or a polymer foam (either 'neat' or fibre reinforced). Syntactic foams (those which are made by distributing hollow microspheres throughout a matrix) are not used as widely as sandwich structure cores, as although they often have greater compressive strength than fibre-reinforced foams, their tensile and shear strengths are usually much lesser [48]. Foam used as a sandwich structure core is the weakest component in the structure, and so is usually the first to fail under static or cyclic loading [42]. The compressive strength of foam is commonly lower than the tensile strength, but the failure mechanism under static and cyclic bending can occur by crack propagation from the tension side [42]. Kanny et al and Kulkarni et al [42, 55] found the cracking occurs at the skin-core interface located at the loading point and propagates towards the support span and kinks to the other side of the skin.

2.7 Polyethylene Surface Treatment

Polyethylene (PE) has particularly low surface energy (30-31 dynes/cm [56]), which manifests as a very poor bonding surface [14, 57-59]. The poor adhesion and incompatibility of PE with other materials (such as pigments, paints , glass fibres, metals, carbon black, and with other polymers) is due to lack of chemical functionality and the semi-crystalline morphology [60]. Common PE surface modification techniques include plasma, flame, corona, photon, electron beam, ion beam, X-ray, and gamma-ray treatments [59]. Corona treatment is limited to simple products such as films. The treatment is often marginal, short lived, and the effluent from corona treatment requires treatment to remove the ozone the process generates [61]. Another PE surface treatment is fluorination (fluorine gas exposure). It significantly improves the bonding ability of PE [62] even with short exposures, due to the introduction of carbonyl groups and acid fluoride functionalities (rather than due to the small increase in surface area from micro-roughness change. Interestingly however, when fluorine is used as a plasma process gas, the opposite effects on wettability can occur [59]). However, fluorine gas is highly toxic and corrosive in very small quantities, and can be fatal if inhaled [63]. Flame treatment is a widely used [56] method for improving polymer surface adhesion. burning an ultra-lean gas mixture creates an ionized oxygen air stream, which alters the polymer surface. Most surface treatments etch the surface and/or add functional molecules (which are more receptive to bonding than molecules on an untreated surface).

The benefits of surface treatment can be quantified by mechanical testing, surface energy testing, or surface chemistry analysis. Mechanically testing is accomplished by such methods as shear testing the interface between a treated surface and a material which is bonded to it. This is a direct method of assessing the bonding improvement. When mechanical testing is not possible, indirect methods of determining the improvement from surface treatment are used. Surface energy testing can be done with methods such as wettability testing (described later, in Section 2.7.2). Another method is surface chemistry analysis, which is the examination of molecules present on the surface of the polymer. This

is achieved with methods such as X-ray photoelectron spectroscopy (XPS) and attenuated total reflection Fourier transform infrared (FTIR-ATR) spectroscopy.

Historical methods of PE surface treatment include mechanical abrasion, solvent wipe, and solvent swell followed by acid or caustic etching [61]. One surface treatment uses a potassium dichromate/sulphuric acid/water solution, which is both carcinogenic and polluting due to the chromate inclusion [64]. Methods involving solvents or acids require expensive disposal systems. Grit or sand blasting to roughen the polymer surface presents health and safety issues, environmental risks, and the benefits are often minimal [61].

2.7.1 Plasma Treatment

Plasma is defined as a state of matter in which a significant number of the atoms and/or molecules are electrically charged or ionized [65], and is known as the fourth state of matter [66]. Plasma surface treatment (or 'plasma treatment' [PT]) is the exposure of a surface to plasma gas. PT is widely popular due to the control of properties produced, low running costs, safety, cleanliness, and because it is a solvent-less process [61]. A common PT setup is shown in Figure 2.17, which involves a part to be treated placed inside an evacuated glass chamber, and a partial vacuum is applied while a selected process gas is introduced and a radio frequency (RF) field is applied (created by the RF coil wound around the chamber). The RF field excites the gas molecules, creating a blend of neutral atoms and reactive radicals formed from free electrons [56], and the resultant glow of the plasma discharge is clearly visible inside the chamber. A typical RF PT setup will have an operating frequency of 13.56 MHz, pressure of 0.1 to 10 Torr, and a process gas flowing at ~ 10cc/min [65].

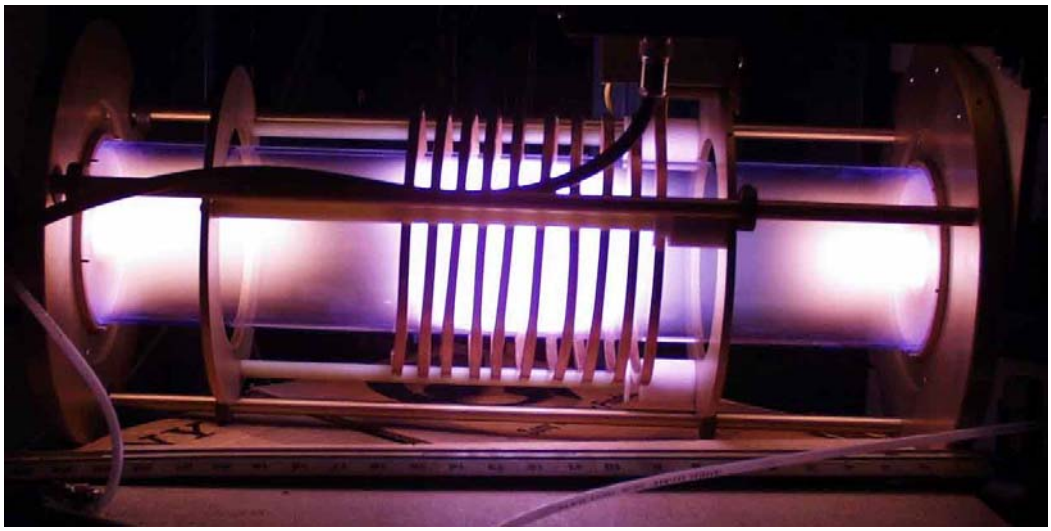

Figure 2.17: PT equipment [67]

PT conducted in a vacuum is not in thermodynamic equilibrium, so the temperature does not rise significantly. This allows the effective treatment of temperature sensitive materials such as LDPE mouldings or fibres [61]. It does not matter how energy is transferred to molecules, so the method of plasma generation also does not matter, provided that equal electron energies and gas temperatures are obtained [65]; consequently, other fields such as microwaves can be used. The PT characteristics can be changed by altering the pressure, charged particle density, applied power, process gases, and temperature (among other factors). Boenig [65] found a considerable number of studies showed a wide variety of free radicals are formed in plasma discharges; those first identified included CH, OH, CN, CS, R-CH, OH, CNO, CNS, CF, CF_2, C_6H_5, NH_2, PH, PH_2, SH, S_2H, and others.

Depending on the type of PT equipment (and various industry terminology) PT is referred to as ‘cold gas plasma surface treatment’, ‘low pressure plasma’, ‘glow discharge plasma’, ‘plasma discharge’, ‘plasma cleaning’, and others. Terms such as ‘glow discharge’ arise because the plasma chamber glows a bright colour when operating (as seen in the photo of some PT equipment, Figure 2.17); similarly the other terms are in relation to the parameters of the PT equipment being used. For simplicity all of these will herein be referred to as ‘plasma treatment’ (PT). Various gases can be used for PT, which are denoted by the name of the gas proceeding ‘PT’ (ie. oxygen PT, argon PT, etc). PT only affects the top layer of a

material, tens of microns thick [68], so the bulk of the material retains its properties.

Oxygen PT modifies polymer surfaces via different reactions, such as hydrogen abstraction, addition to a double bond, and by entry into a C-H or C-C bond. It is generally assumed that the main reaction is the addition of oxygen to a double bond, thus forming epoxides, carbonyl, carboxyl, ether, peroxide, and other functional groups during PT [65, 69, 70]. Kaplan and Rose [61] reported the species found in an oxygen plasma include O^+, O^-, O_2^+, O_2^-, O, O_3, ionized ozone, metastably-excited O_2, and free electrons. When the components recombine, they emit energy, photons, and UV radiation. The photons have enough energy to break the polymer's carbon-carbon and carbon-hydrogen bonds [61]. Oxygen PT has been found to improve the wettability of PE [69, 70] and it requires less time/power than argon PT for similar improvements to wettability [70], but Dayss et al [58] found excessive oxygen PT decreased the wettability after a certain time period.

Lehocky et al [69] found air PT improved the wettability of PE, with only short treatment times (around one minute). Carbonyl, carboxyl, ether, peroxide, and other functional groups were created on the polymer surface (detected by attenuated total reflection accessory [ATR] fourier-transform infrared spectroscopy [FTIR] and x-ray photoelectron spectroscopy [XPS] analysis).

Argon PT has been shown to improve the wettability of PE, after short treatment times [68, 70]. Argon PT activates the surface of PE, so when the sample is exposed to air, the surface adsorbs moisture and therefore receives a post treatment functionalisation [70]. Svorcik et al [68] found argon PT lead to ablation of PE surface layers, around 1 micrometer thick. The post-treatment surfaces were found to have been oxidised, with carbonyl, carboxyl and amide groups present, together with C=C bonds either in aromatic or in aliphatic structures. The surface morphology (roughness) increased dramatically after PT. The relation between the length of the PT time and the degree of aging (or loss of effectiveness) of the PT have been shown by Svorcik et al [68]. Long exposures (between 50 and 400 seconds) of PE to argon PT increased the wettability with

increasing PT time when tested 10 seconds after PT, but when the contact angle was tested 386 hours after argon PT, the wettability decreased in relation to the original PT time. Therefore, the elapsed time after PT before a sample is used or adhered to is an important factor when developing a PT application. Guruvenket et al [70] observed that prolonged treatment or too high power levels deteriorated the polymer surface. Shi et al [71] studied of the surface chemistry effects of argon PT applied to LDPE. ATR-FTIR spectroscopy showed peroxide bonds were formed. This is from the reaction of free radicals (formed during treatment with oxygen) and water in the air (when exposed to these after treatment). It was also concluded that C=C bonds were formed by the reaction of free radicals (from plasma etching and hydrogen abstraction).

Nitrogen PT is widely known to improve the wettabilty of PE surfaces [59], by incorporating oxygen functionalities both during and after the PT. This is due to free radicals which are created on the polymer surface and react with oxygen when the surface is exposed to air [59].

2.7.2 Wettability Analysis

Two popular methods used to measure wettability of polymers are water contact angle measurement and dyne pen analysis. Wettability is related to a materials surface tension and has units of dyne/cm or mN/m, which is equivalent to mJ/m^2 surface free energy [72]. It is known to be an important characteristic that relates to the adherence of dyes, inks, and adhesives to a material [65]. The water contact angle phenomenon was first noticed by Young [73].

Water contact angles can be determined by finding the angle between the solid surface and a line tangent to the water drop surface, at the base of the drop. This is usually done using a goniometer. This is a simple device that illuminates a drop of water so that a silhouette is visible through a viewing lens and a reference line is positioned to show the contact angle. Industries which closely monitor wettability often use automated contact angle measurement equipment. Pure water is commonly used as the test liquid. It has a surface tension of 72 mN/m. Water

contact angles decrease with increasing surface energy [61], so low contact angles indicate a greater tendency for the liquid to wet a solid and large contact angles are associated with poor wettability [72].

Force balance or equilibrium at the solid-liquid boundary is given by Young's equation (equation 5) for contact angles greater than zero (where θ is the contact angle [shown in figure 2.18], and γ_{lv}, γ_{sv} and γ_{sl} are the surface free energies of the liquid-vapour, solid-vapour and solid-liquid interfaces, respectively).

$$\gamma_{lv} \cos\theta = \gamma_{sv} - \gamma_{sl} \qquad \text{(equation 5)}$$

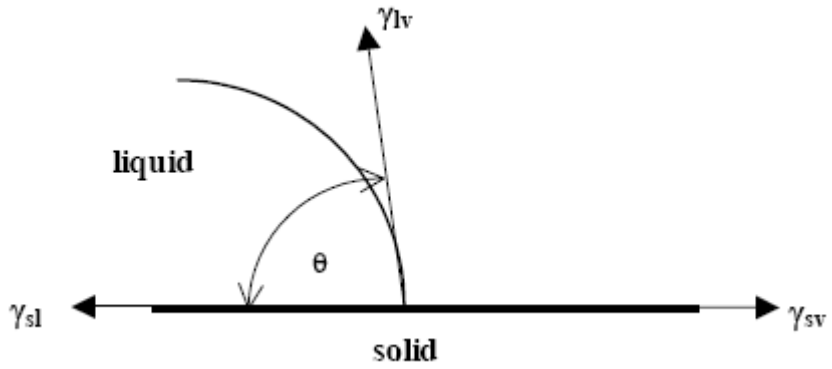

Figure 0.18: Water contact angle diagram [72]

Young's equation would suggest there is a define water contact angle for any solid/liquid/gas system, but this has been shown to be untrue due to the complex mechanisms involved in phase interfaces. No contact angle approach as yet allows the determination of solid surface tensions from such angles [72, 74]. It has been found that for a given system, a number of stable angles can be measured, and factors such as surface roughness, heterogeneity, and contaminants will affect the contact angle measurements [75]. Water contact angles are useful however, for comparative testing of surfaces when the same testing conditions are used.

Dyne pens are a series of pens with incremental varying and known surface tensions, which are used in sequence by applying liquid to a surface, then examining which one just wets the surface (as opposed to breaking up into drops). Although simple to use, they are less popular due to the limited shelf life and possible inaccuracy from contamination which can occur from repeated use.

2.8 Environmental Issues

2.8.1 The Economics of Being Environmentally Aware

Shrivastava [76] has shown that businesses which integrate environmental technologies and strategies can benefit in multiple ways. These include cost reduction, revenue enhancement, improving supplier ties, quality improvement, development of a competitive edge, reduction of liabilities, social and health benefits, improved public image, and staying ahead of the regulatory curve. Minimising energy use, decreasing waste material, and using alternate methods to chemical treatments can decrease costs, and the development of 'environmental technologies' can allow entry into growing markets. Companies which are seen to be socially and environmentally responsible can often gain a competitive edge [76]. This is due to customer satisfaction resultant from the knowledge that the company they are purchasing from is environmentally aware and operates in a socially responsible manner. The Body Shop is a famous example of a successful, environmentally aware business [76]. This 'clean and green' image is particularly important for New Zealand (NZ) companies, to align with NZ tourism and food industries marketing NZ and its products to the world. An example of how NZ is marketed is shown by the banner in Figure 0.19, which is from the worldwide marketing campaign, '100% pure New Zealand'. This campaign has been running since 1999.

Figure 0.19: '100% Pure New Zealand' banner [77]

An example of companies profiting from environmental awareness is 3M Corporation. They have successfully implemented many environmentally friendly practices, processes and products. Their 'Pollution Prevention Pays Program', or '3P Program' is used to chose projects which must eliminate or reduce pollutants, benefit the environment through reduced energy use or manufacturing efficiency, be technologically innovative, and save money or increase sales. Between 1975 and 1989 the 3P Program reduced manufacturing pollution by half and saved the company US$500 million in costs [76]. The link between environmental and economic performance has been widely debated recently [78], so financial benefit from being environmentally proactive is not guaranteed in all or any circumstances.

2.8.2 Recycling

In 2004 in the United States alone, 2.5 billion kg of polyurethane (all types) was produced. When the products containing this material end their useful lives, they will likely either be disposed of in a landfill or recycled in some way. Disposing of PU is common practice, as PU-based products usually do not have any adverse effects on landfills (such as degradation or leaching), but recycling is another option. Unfortunately rigid thermoset polyurethane foam cannot be melted and re-formed like thermoplastics can, so other methods are used to recycle and/or re-use it. The waste PU processing method will depend on factors such as the pre-processed material properties, the applications available for it, the availability of recycling or re-processing equipment, and logistical, legal, economic and ecological factors. The three main methods used for recycling rigid PU are mechanical recycling, feedstock recycling, and energy recovery. Mechanical recycling includes using crushed PU with processes such as adhesive pressing, particle bonding, regrinding, injection moulding, or compression moulding. This produces items such as pressed particle boards (for doors and walls on ships and buildings etc). Ground-down PU can also be used as an oil spill absorbing material [79]. Feedstock recycling uses a series of chemical and/or thermal processes to break the polymer down into low molecular fragments; this includes glycolysis (which produces polyols from process and post-consumer PU scrap by

reacting polyurethanes with diols at high temperatures), hydrolysis (a reaction of polyurethane with water, can produce polyols and amine intermediates from PU process and post-consumer scrap), pyrolysis (uses a heated, oxygen-free environment to break down PU into gas and oil), and hydrogenation (takes pyrolysis one step further to produce pure gases and oils through a combination of heat, pressure and hydrogen) [41, 79]. 'Recycling' by energy recovery is the process of incinerating PU to heat another process. This is undertaken in rotary kilns, fluidized beds, two-stage incineration, high temperature gasification, or municipal solid waste combustion. Modern incinerators can recover energy in an environmentally safe manner, using flue-gas scrubbers [79].

2.8.3 Ozone Depletion

In the mid 1980s it was discovered that certain chlorofluorocarbons (CFCs) used as chemical blowing agents (CBAs) for polymer foams were thought to help cause depletion of the ozone layer and contribute to global warming [41]. Hydrochlorofluorocarbons (HCFCs) were developed as a replacement, but are now thought to also affect the ozone layer, so are currently being phased out. Most foam systems commonly use chemical blowing agents, and CFCs and HCFCs are popular CBAs due to their low thermal conductivity and good processing ability. Although CFCs and HCFCs are still used in many places around the world, there are efforts to faze them out and find new CBAs with similar or better properties, which don't deplete the ozone layer. Some foam suppliers have already developed alternatives with thermal conductivity properties equivalent to those available with current HCFC technology [80]. The European community stopped use of HCFCs for PU foam production in 1993, and most other developed countries are following with limits and plans to phase out ozone depleting substances, in accordance with The Montreal Protocol on Substances That Deplete the Ozone Layer. The 'Montreal Protocol' is an international agreement that sets standards to prevent further damage to the stratospheric ozone layer. The treaty was originally signed in 1987 and substantially amended in 1990 and 1992. It stipulates that the production and consumption of compounds that deplete ozone in the stratosphere (chlorofluorocarbons, halons, carbon

tetrachloride, and methyl chloroform) were to be phased out by 2000 (2005 for methyl chloroform) [81].

2.8.4 Other Developments

Another environmentally friendly development is the production of bio-derived polyols, to replace petroleum-based polyether and copolymer polyols [41, 82]. The starting material is a renewable resource and does not directly rely on fossil fuel for synthesis.

2.9 Literature Review Bibliography

1. Knoth, P., A. Pfitzmannn, and e. al. *society of plastics engineers*. in *antec*. 2003.
2. Crawford, R., *Vice Chancellor, University of Waikato (Hamilton, NZ)*. 2008.
3. *Rotational moulding website*. [cited; Available from: www.rotationalmoulding.ca.
4. R.J. Crawford and M.P. Kearns, *Practical Guide to Rotational Moulding*. 2003: Rapra Technology.
5. *Coastline Plastics*. [cited; Available from: www.coastlineplastics.com.au.
6. [cited; Available from: www.polivinil.com.
7. Mooney, D.P., *Custom Plastics Research*. 2005.
8. *Jacksonkayak website*. [cited; Available from: www.jacksonkayak.com.
9. *cree website*. [cited; Available from: www.cree.cr.
10. *Gallagher website*. [cited; Available from: www.gallagher.co.nz.
11. *gnr8.biz*. [cited; Available from: www.gnr8.biz.
12. Callister, W., *Materials Science and Engineering an Introduction*. 6 ed. 2003: John Wiley & Sons, Inc.
13. *chemicals-technology.com*. [cited; Available from: www.chemicals-technology.com.
14. Muzzy, J.D., *Thermoplastics - Properties.* Comprehensive Composite Materials, 2000. **2**: p. 57-76.
15. Yan, W., R.J.T. Lin, and D. Bhattacharyya, *Particulate reinforced rotationally moulded polyethylene composites - Mixing methods and mechanical properties.* Composites Science and Technology, 2006. **66**(13): p. 2080-2088.
16. Torres, F.G. and C.L. Aragon, *Final product testing of rotational moulded natural fibre-reinforced polyethylene.* Polymer Testing, 2006. **25**(4): p. 568-577.
17. F.G. Torres and R.M. Diaz, *Morphological Characterisation of Natural Fibre Reinforced Thermoplastics (NFRTP) Processed by Extrusion, Compression and Rotational Moulding.* Polymers and Polymer Composites, 2004. **12**(8): p. 705-718.
18. Lee, S.M., *Handbook of Composite Reinforcements*. 1993, California: Wiley-VCH.
19. M.F.Ashby and D.R.H.Jones, *Engineering Materials 2*. 3 ed. 2006, Oxford: Butterworth-Heinemann
20. Wu, H.F., D.W. Dwight, and N.T. Huff, *Effects of silane coupling agents on the interphase and performance of glass-fiber-reinforced polymer composites.* Composites Science and Technology, 1997. **57**(8): p. 975-983.
21. Abdel-Magid, B., et al., *Flexure creep properties of E-glass reinforced polymers.* Composite Structures, 2003. **62**(3-4): p. 247-253.
22. Kelly, A. and W.R. Tyson, *Tensile properties of fibre-reinforced metals: Copper/tungsten and copper/molybdenum.* Journal of the Mechanics and Physics of Solids, 1965. **13**(6): p. 329-338.
23. Beckermann, G., *Performance of Hemp-Fibre Reinforced Polypropylene Composite Materials*. 2007, University of Waikato: Hamilton.

24. Fu, S.-Y. and B. Lauke, *Effects of fiber length and fiber orientation distributions on the tensile strength of short-fiber-reinforced polymers.* Composites Science and Technology, 1996. **56**(10): p. 1179-1190.
25. Bowyer, W.H. and M.G. Bader, *On the reinforcement of thermoplastics by imperfectly aligned discontinuous fibres.* Journal of Materials Science, 1972. **7**(11): p. 1315-1321.
26. Kalaprasad, G., et al., *Theoretical modelling of tensile properties of short sisal fibre-reinforced low-density polyethylene composites.* Journal of Material Science, 1997. **32**(16): p. 4261-4267.
27. Thomason, J.L., et al., *Influence of fibre length and concentration on the properties of glass fibre-reinforced polypropylene: Part 3. Strength and strain at failure.* Composites Part A: Applied Science and Manufacturing, 1996. **27**(11): p. 1075-1084.
28. Klempner, D. and K.C. Frisch, *Handbook of Polymeric Foams and Foam Technology*. 1991, New York: Hanser.
29. Kulshreshtha, A.K. and C. Vasile, *Handbook of Polymer Blends and Composites*. Vol. 1. 2002.
30. Dwight, D.W., K. Anthony, and Z. Carl, *Glass Fiber Reinforcements*, in *Comprehensive Composite Materials*. 2000, Pergamon: Oxford. p. 231-261.
31. Gibson, L.J. and M.F. Ashby, *Cellular Solids - Structure and Properties*. 2nd ed. 1997, Cambridge: Cambridge University Press.
32. Saint-Michel, F., et al., *Mechanical properties of high density polyurethane foams: I. Effect of the density.* Composites Science and Technology, 2006. **66**(15): p. 2700-2708.
33. Kabir, M.E., M.C. Saha, and S. Jeelani, *Tensile and fracture behavior of polymer foams.* Materials Science and Engineering: A, 2006. **429**(1-2): p. 225-235.
34. Saha, M.C., et al., *Effect of density, microstructure, and strain rate on compression behavior of polymeric foams.* Materials Science and Engineering: A, 2005. **406**(1-2): p. 328-336.
35. Christensen, R.M. and K.H. Lo, *Solutions for effective shear properties in three phase sphere adn cylinder models.* J.Mech.Phys.Solids, 1979. **27**: p. 315-330.
36. Harding, R.H.J., *Morphologies of Cellular Materials. Resinography of Cellular Plastics.* Cellular Plastics, 1965. **1**: p. 385.
37. Quinn, S., *Chemical blowing agents: providing production, economic and physical improvements to a wide range of polymers*, in *Plastics Additives & Compounding*. May 2001.
38. Bush, S.F. and O.K. Ademosu, *Low-density rotomoulded polymer foams.* Colloids and Surfaces A: Physicochemical and Engineering Aspects, 2005. **263**(1-3): p. 370-378.
39. Lawrence, R., *Industrial Technical Solutions (Tauranga, NZ)*. 2006.
40. *dunagroup website*. [cited; Available from: www.dunagroup.com.
41. *polyurethane.org*. [cited; Available from: www.polyurethane.org.
42. Kanny, K., et al., *Dynamic mechanical analyses and flexural fatigue of PVC foams.* Composite Structures, 2002. **58**(2): p. 175-183.
43. Subhash, G., Q. Liu, and X.-L. Gao, *Quasistatic and high strain rate uniaxial compressive response of polymeric structural foams.* International Journal of Impact Engineering, 2006. **32**(7): p. 1113-1126.

44. Saint-Michel, F., L. Chazeau, and J.-Y. Cavaille, *Mechanical properties of high density polyurethane foams: II Effect of the filler size.* Composites Science and Technology, 2006. **66**(15): p. 2709-2718.
45. Mahfuz, H., et al., *Fabrication, synthesis and mechanical characterization of nanoparticles infused polyurethane foams.* Composites Part A: Applied Science and Manufacturing, 2004. **35**(4): p. 453-460.
46. Cao, X., et al., *Polyurethane/clay nanocomposites foams: processing, structure and properties.* Polymer, 2005. **46**(3): p. 775-783.
47. Alperstein, D., M. Narkis, and S. Kenig, *Effect of Particulate Reinforcement on Creep Behaviour of Polyurethane Foams.* Polymer Composites, 1984. **5**(2): p. 155-158.
48. Alonso, M.V., M.L. Auad, and S. Nutt, *Short-fiber-reinforced epoxy foams.* Composites Part A: Applied Science and Manufacturing, 2006. **37**(11): p. 1952-1960.
49. T.C. Cotgreave and J.B. Shortall, *The mechanism of reinforcement of polyurthane foam by high-modulus chopped fibres.* Journal of Material Science, 1977. **12**(4): p. 708-717.
50. Huang, Y.-J., L. Vaikhanski, and S.R. Nutt, *3D long fiber-reinforced syntactic foam based on hollow polymeric microspheres.* Composites Part A: Applied Science and Manufacturing, 2006. **37**(3): p. 488-496.
51. Shen, H. and S. Nutt, *Mechanical characterization of short fiber reinforced phenolic foam.* Composites Part A: Applied Science and Manufacturing, 2003. **34**(9): p. 899-906.
52. Shen, H., S. Nutt, and D. Hull, *Direct observation and measurement of fiber architecture in short fiber-polymer composite foam through micro-CT imaging.* Composites Science and Technology, 2004. **64**(13-14): p. 2113-2120.
53. *ASTM C274-53*, American Society for Testing Materials.
54. *tricelcorp website*. [cited; Available from: www.tricelcorp.com.
55. Kulkarni, N., et al., *Fatigue crack growth and life prediction of foam core sandwich composites under flexural loading.* Composite Structures, 2003. **59**(4): p. 499-505.
56. *Accudynetest website*. [cited; Available from: www.accudynetest.com.
57. Lai, J., et al., *Study on hydrophilicity of polymer surfaces improved by plasma treatment.* Applied Surface Science, 2006. **252**(10): p. 3375-3379.
58. Dayss, E., G. Leps, and J. Meinhardt, *Surface modification for improved adhesion of a polymer-metal compound.* Surface and Coatings Technology, 1999. **116-119**: p. 986-990.
59. Chan, C.M., T.M. Ko, and H. Hiraoka, *Polymer surface modification by plasmas and photons.* Surface Science Reports, 1996. **24**(1-2): p. 1-54.
60. Chung, T.C., *Functionalization of Polyolefins*. 2002: Elsevier.
61. Kaplan, S.L. and P.W. Rose, *Plasma Surface Treatment of Plastics to Enhance Adhesion.* Int.J.Adhesion and Adhesives, 1991. **11**(2): p. 109-113.
62. Kranz, G., et al., *The effect of fluorination on the surface characteristics and adhesive properties of polyethylene and polypropylene.* International Journal of Adhesion and Adhesives, 1994. **14**(4): p. 243-253.
63. *MSDS*. [cited; Available from: www.ptcl.chem.ox.ac.uk
64. Rosty, R.e.a. *Surface Preparation of Polyolefins Prior to Adhesive Bonding*. in *32nd International SAMPE Symposium*. 1987. Anaheim, California.

65. Boenig, H.V., *Plasma Science and Technology*. 1982, Ithaca and London: Cornell University Press.
66. Crookes, W. *On a Fourth State of Matter*. in *Proceedings of the Royal Society of London*. 1880.
67. *Manitausys website*. [cited; Available from: www.manitousys.com.
68. Svorcik, V., et al., *Modification of surface properties of high and low density polyethylene by Ar plasma discharge.* Polymer Degradation and Stability, 2006. **91**(6): p. 1219-1225.
69. Lehocky, M., et al., *Plasma surface modification of polyethylene.* Colloids and Surfaces A: Physicochemical and Engineering Aspects, 2003. **222**(1-3): p. 125-131.
70. Guruvenket, S., et al., *Plasma surface modification of polystyrene and polyethylene.* Applied Surface Science, 2004. **236**(1-4): p. 278-284.
71. Shi, L.-S., L.-Y. Wang, and Y.-N. Wang, *The investigation of argon plasma surface modification to polyethylene: Quantitative ATR-FTIR spectroscopic analysis.* European Polymer Journal, 2006. **42**(7): p. 1625-1633.
72. Duncan, B., et al., *Techniques for characterising the wetting, coating and spreading of adhesives on surfaces*. 2005, National Physics Laboratory United Kingdom.
73. Young, T., *An Essay on the Cohesion of Fluids.* Philosophical Transactions, 1805. **95**: p. 65-87.
74. Kwok, D.Y. and A.W. Neumann, *Contact angle interpretation in terms of solid surface tension.* Colloids and Surfaces A: Physicochemical and Engineering Aspects, 2000. **161**(1): p. 31-48.
75. Matijevic, E., *Surface and Colloid Science*. Vol. 2. 1969, New York: Wiley - Interscience.
76. Shrivastava, P., *Environmental Technologies and Competitive Advantage.* Strategic Management Journal, 1995. **vol 16, Special Issue: Technological Transformation and the New Competitive Landscape**: p. 183-200.
77. *pointofview.net.nz*. [cited; Available from: www. pointofview.net.nz.
78. Schaltegger, S. and T. Synnestvedt, *The link between 'green' and economic success: environmental management as the crucial trigger between environmental and economic performance.* Journal of Environmental Management, 2002. **65**: p. 339-346.
79. Brandrup, et al., *Recycling and Recovery of Plastics*. 1995: Hanser.
80. *Baxenden Chemicals Limited*. [cited; Available from: www.baxchem.co.uk.
81. *ciesen website*. [cited; Available from: www.ciesin.org.
82. *bioh.com*. [cited; Available from: www.bioh.com.

Chapter 3 – Experimental Design

3.1. Chapter Overview

This chapter begins with descriptions of the specific materials used in this research project, including RIM PU foam, glass fibre, rotomoulding PE, and particles for increasing the foam/skin interfacial strength.

Tensile testing was undertaken to attain tensile strength and modulus of the foam, for use in engineering design, and to compare the reinforced specimen strength results with theoretical models. Creep properties of the foam were tested because the product may endure elevated temperatures and constant loads, and if it undergoes creep deformation, it will be considered a failure. Foam impact testing was undertaken because the product may receive impact loads, which are only partially absorbed by the rotomoulded skin. Rotomoulded PE cuboids were produced with various secondary particles added to the polymer charge, which were found to migrate to the inner surface during processing and provide a rough inner surface. It was hypothesised that when these cuboids were foam-filled, a mechanical interlocking effect would result between the skin and the foam core, due to the embedded particles. This may overcome issues from the lack of bonding between the two polymers and possibly improve product performance. Interfacial shear testing of sections of foam-filled cuboids was performed to determine the interfacial shear strength. Specimens cut from rotomoulded PE were plasma treated to assess the possible improvements to surface wettability, which may correspond to an improvement of the foam/skin interfacial strength. Air was chosen for the plasma treatment process gas. It comprises of 78.08% nitrogen, 20.95% oxygen, 0.93% argon, (plus 0.04% of other gases - mainly carbon dioxide [1]). Air is known as an effective plasma process gas for PE wettability improvement, is readily available in all parts of the world, and the cost compares favourably to other common plasma process gases (air: \$0.00/m^3, oxygen: \$11.03/m^3 [2], argon: \$31.10/m^3 [2], nitrogen: \$10.33/m^3 [2]. Costs are New Zealand dollars, excluding Goods and Services Tax, GST). The rotomoulded

PE surface wettability was analysed before and after treatment, with water contact angle testing.

Fibre orientation, cell morphology, density variations and voids were examined using various imaging techniques, including both the light box method for thin (<6mm) sheets of foam and X-ray for foam samples which were thicker. Scanning electron microscopy (SEM) was used microscopic examination of failed tensile specimen fracture surfaces.

3.2. Materials

3.2.1. Reaction Injection Moulding Polyurethane (RIM PU) Foam

Isofoam RM6291W (RIM PU, produced by Baxenden Chemicals Limited) was the foam system used for this research project. It is a two component (resin and isocyanate) system, which when mixed, reacts and foams to form rigid structural foam. The components are mixed at a ratio of 40% resin and 60% isocyanate by weight. At 20°C the resin component of the foam has a viscosity of 1600-2600 Pa.s and specific gravity of 1.07, and the Isocyanate component (a liquid grade of crude diphenylmethane di-isocyanate [MDI]) has a viscosity of 300-400 mPa.s and specific gravity of 1.24. The free rise core density is 107kg/m^3 and typical closed-moulded densities are 175-700kg/m^3. The foam system has a cream time of 38 seconds, gel time is 75 seconds, and free rise time of 111 seconds [3], however, the reaction speed can be altered by changing the material temperature; increasing the component materials' temperature by 10°C decreases the materials' viscosity but doubles the reaction rate [4]. The supplier-recommended mould temperature range for optimal processing is 50-60°C and the ideal material temperature for storage and use is 20°C. The approximate cost of the foam in manufacturing quantities is $9.75/kg (NZD+gst). The foam components were stored at room temperature and placed in a temperature controlled chamber at 20°C for at least 2 hours before use. Foam components (and their measuring cups – pre and post-use) were weighed with 2kg electric platform scales, accurate to +/- 1g.

3.2.2. Glass Fibre

Two fibre types were used for reinforcing the foam. The first type was Owens Corning 'ME1020' fibre roving (continuous fibre). This was recommended as the most suitably sized fibre available for the RIM PU foam being used [5]. Manufacturing quantities of ME1020 fibre would cost approximately $1.70/kg (NZD+gst) [6]. The ME1020 roving was chopped to 6mm lengths with a hand-held air powered chopper gun (model: 171-A, produced by Fibre Glast Developments Corporation [7], as shown in figure 3.1). The chopper gun required modification to cut through the roving fully, including replacement of the rubber wheel (which acts against the blades to cut the fibres) with one made from solid PU and use of a 13mm (internal diameter) air hose, to provide enough flow to power the chopper gun without stoppages.

Figure 3.1: Air powered chopper gun

The second fibre type was Owens Corning '101C' 6mm chopped strand fibre. It is sized to suit unsaturated polyester, epoxy, and phenolic matrices, and commonly used for bulk moulding compounds (BMCs). Manufacturing quantities would cost approximately $5.50/kg (NZD+gst) [8].

Fibre was weighed with a Satrue 'High Performance Pocket Scale' (model: SD-H2100, accurate to 0.01g). Disposable gloves were worn when handling fibre, to prevent surface contamination.

3.2.3. Rotomoulding Polyethylene (PE)

Metallocene based rotomoulding-specific linear high density polyethylene (HDPE) powder, 'Cotene 3979' grade (made by ICO Polymers [9]), was used for all rotomoulded samples. This standardised PE is available in many colours, but only powders with blue and green pigments were used for testing. Cotene 3979 is marketed as a material with high density, stiffness, and excellent impact strength, and some typical applications include surf skis and performance kayaks [9]. It has a melt flow index (MFI) of 4.5g/10min [9], and manufacturing quantities would cost approximately $6.15/kg (NZD+gst) [10]. When annealed, it has an ultimate tensile strength (UTS) of 23.1MPa [10], tensile modulus of 1300MPa [10], flexural modulus of 980MPa [10], impact strength of 19.8kJ/m^2 [10], and density of 0.947g/cc [9]. All rotomoulding for this research project was undertaken using a small 'research and development' oven, which had monitoring of internal and external mould temperatures, process time, and rotation speed, for accurate processing.

3.2.4. Particles for Foam/Skin Interfacial Shear Strength Modification

The particles trialled for the interfacial shear strength modification included:

- Aluminium oxide (Al_2O_3): '8 grit' (2-2.8mm particle size). ($3.85/kg)
- Spherical glass beads: Potters AH grade (90 - 45 microns). ($1.92/kg)
- Silica. (average particle diameter 20 microns). ($2.00/kg)
- Silicon carbide: (average particle size 46.5 - 42.5 microns). ($12.00/kg)
- Vulkan Chronital spherical austenitic stainless steel shot. (particle size >0.2mm). ($13.52/kg),
- Steel grit (H6-18, 1-1.4mm). ($22.64/kg),
- Crushed walnut shell. (1.9-3mm) ($3.02/kg)
- 6mm chopped glass fibre. ($5.50/kg)
- 12mm chopped glass fibre. ($5.50/kg)

Particles were procured from Syntech Distributors Ltd (Auckland, New Zealand), except for glass fibre, which was from The Fibreglass Shop (Hamilton, New Zealand) [8]. Prices are NZD+GST.

3.3. Foam Processing

3.3.1. Discussion of Foam Mould Development

Early trial moulding of RIM PU foam used various moulds in attempt to directly produce test specimens, but this was found to be inefficient, due to difficulty accurately mixing small volumes of the foam components. 10mm PE sheet was used for the foam mould surface material. Due to the low surface energy of PE (discussed in Section 2.7), minimal release agent would be required. Testing showed the foam released easily from smooth PE sheet when wax mould release agent was used, but the foam would adhere to machined PE surfaces. Moulds which dismantled into multiple pieces after moulding were found to be more successful than two piece moulds. A multi-layer mould was constructed to produce a variety of different size foam blocks or sheets, depending on which inner sections of the mould were used. The mould sizes available included 293x200x6mm, 200x300x3.2mm, 230x110x26mm, and 200x 300x12mm. Test specimens were cut or machined from these larger samples. The moulds were externally strengthened with two sheets (per side) of 18mm medium density fibreboard (MDF), and secured together with 12 bolts.

3.3.2. Laboratory Foam Processing Equipment

A laboratory processing system was designed and constructed to allow timely mixing and injection of the two foam components into the mould. It consisted of a mixing cup (80mm diameter) with a pneumatic ram powered movable base, which acted like the plunger of a syringe. A frame was built so that the mould could be

easily and accurately lowered onto the mixing cup (as shown in Figures 3.2, 3.3, and 3.6). When the mould was raise it sealed the mould heating chamber. An attachment was made for the mould, which sealed over the top of the mixing cup when the mould was lowered. The maximum injection hole size between the mixing cup and the mould was specified by the rotomoulding company this research was for, to be 8mm (because the maximum hole size in a product is 10mm and an injection tube may have up to a 1mm wall thickness).

Figure 3.2: Foam processing - mould down

Figure 3.3: Foam processing - mould up

A Sanyo (model: SHM-X110) electric kitchen mixer was used to mechanically mix the two components of the RIM PU foam system (and fibre). The twin mixing head design and high mixing speed was suitable for this application, but the mixing attachments required extending to reach the base of the mixing cup (the mixing heads are shown in Figures 1.2 and 1.3). To minimise mixing time, the maximum mixing speed was used ('level 5' plus the 'burst' function). The speed of the mixers were found to be 1190rpm (+/-20rpm) at this speed, measured with a laser rpm measurer (model: SHMPO DT-205L). The mixing quality and the ability to inject the foam into the mould was largely a function of mixing time. 20 seconds after initial mixing the viscosity was too high to inject the foam into the mould, but, if the foam was insufficiently mixed, the foam would be unsuitable for use. Trial and error found the optimum mixing procedure to be 10

seconds with the electric mixer (while moving it around the mixing cup in a circular fashion), plus 4-5 seconds using a spatula (to mix any material that the electric mixer may have missed).

Figure 3.4: Twin mixing heads

Figure 3.5: Mixing head showing size

Figure 3.6: Mixing cup and equipment frame

The mixed foam components were injected upward into the base of the mould and displaced air while foaming upward. To allow for this, a vent hole was placed in the top of the mould, with a plug used to block the vent hole when the foam reached it. Various methods were trialled for the vent and plug, but the final setup involved an M12 threaded hole (in the top of the mould), and a high-tensile bolt used as the vent hole plug. The plug was installed and removed with a ratchet and socket.

Due to compression of the inner layer of the mould when it was bolted together, the mould volumes were found to be less than anticipated, so these were determined by measuring the amount of water which they took to fill. These values were used with the data on specific gravity of the foam components and the foam target density, to calculate the required weight of each foam component to mix and inject into the mould. Also, the losses from the measuring cups and processing equipment were determined experimentally, and accounted for in the foam component mix weight calculations. Foaming RIM PU creates high internal mould pressure due to the creation of the gas phase in the material, and it was found that due to this, any foam which was not adequately sealed and contained within the mixing cup and mould would escape readily during the injection phase, so there was often loss of foam during sample preparation. To account for this variation between samples and to accurately report foam performance, the density of samples was determined experimentally after it was produced. This was achieved by the water displacement method (dividing the sample weight by its volume, determined by the amount of water it displaces in a measuring container), or by dividing the sample weight by its calculated volume (length x width x height).

To heat the mould to the required range, an insulated temperature-controlled heating chamber was designed and built (as seen in Figures 1.2 and 1.3). A small electric fan heater was used to heat the mould chamber. This was controlled by a Yamatake-Honeywell SDC20 Electronic Temperature Controller. Due to the low thermal conductivity of the mould, the heat transfer from the heating chamber to the inner mould surface was slow, restricting foam production. To increase the heating rate, heating elements were installed into the mould in slots cut in the

MDF sheets. This was also controlled by a Yamatake-Honeywell SDC20 Electronic Temperature Controller. There was a sufficient length of wire between the two main sections of the mould to allow for ease of dismantle and re-assembly. Steel angle section was added to the mould to limit the deflection from to the force of the expanding foam. An exploded view of the mould is shown in Figure 1.7. The outermost parts are the steel reinforcements, the thick blocks are MDF sheets, then in between them are the PE sheets and the inner mould parts, which determine what size sample is made (The mould entry and vent holes and the heating elements are not shown on this picture).

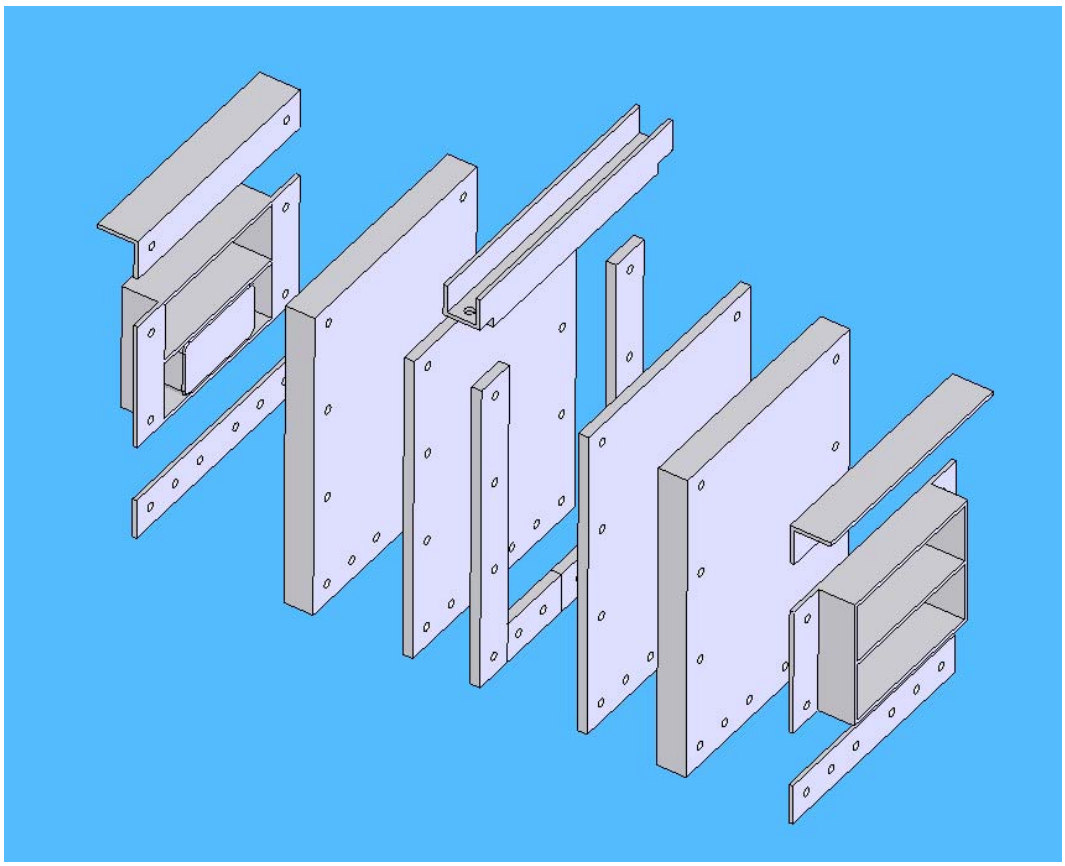

Figure 3.7: Exploded diagram of mould

3.3.3. RIM Equipment Cleaning

RIM PU foam was found to be particularly difficult to remove from most surfaces it contacted during processing. Cleaning the mixing cup, plunger and other components was attempted using solvents (methylene chloride, acetone, and mirotone), but were found to be slow, messy, and less effective than mechanical

scraping of the cured foam. Applying mould release wax ('Nu Age' brand [8]) to surfaces contacting the foam aided the cleaning process. Cured foam (post-moulding) in the injection hole (between the mixing cup and the mould) required drilling to remove. The foam was stronger than the PE which the part was made from so the injection hole alignment was effected by the drilling. A tubular steel insert was installed to remedy this. The electric mixer attachments and vent hole plug were cleaned after each use, using a high speed wire wheel, and the vent hole thread required re-tapping after each use.

3.3.4. Laboratory Foam Production Method

The following method was employed to produce foam samples:

1. Wax release agent was applied to all required surfaces,
2. The mould was assembled and attached to the process equipment frame swing arm,
3. The speed and operation of the mixing cup base movement was checked, and if necessary the speed was adjusted prior to use by altering the pressure level of the air compressor or air valve. These allowed for changes in friction and other variables, so that each injection was approximately the same (approximately 3 seconds),
4. The appropriate amounts of resin and isocyanate components were weighed into paper cups,
5. The resin was poured into the mixing cup (and if a reinforced foam sample was being made, fibre was also added),
6. The isocyanate component was poured into the mixing cup,
7. The components were mixed for 10 seconds with the electric mixer (timed with a stopwatch),
8. The spatula was used for final mixing, for 4-5 seconds,
9. The mould was lowered onto the top of the mixing cup and clamped down,
10. The mixing cup base pneumatic ram was activated, to inject the foam into the mould,
11. When the foam reached the vent hole at the top of the mould, the vent hole plug was installed,

12. After two minutes, the vent hole plug bolt was removed, the mould was raised from the mixing cup, and the remaining foam in the mixing cup was cleaned out,
13. The mixing cup base was cycled up and down multiple times to aid cleaning of the mixing cup,

3.4. Tensile Testing

3.4.1. Equipment

An Instron 4204 universal test machine was used for tensile testing, with a 5kN load cell. An extensometer was clipped to each specimen to measure the strain during testing (as shown in Figure 1.4). The width and thickness of each specimen was measured at multiple points along the gauge length and the average values were entered into the test equipment to allow strength and modulus calculation. The speed of testing was 5mm/min and continued until failure occurred.

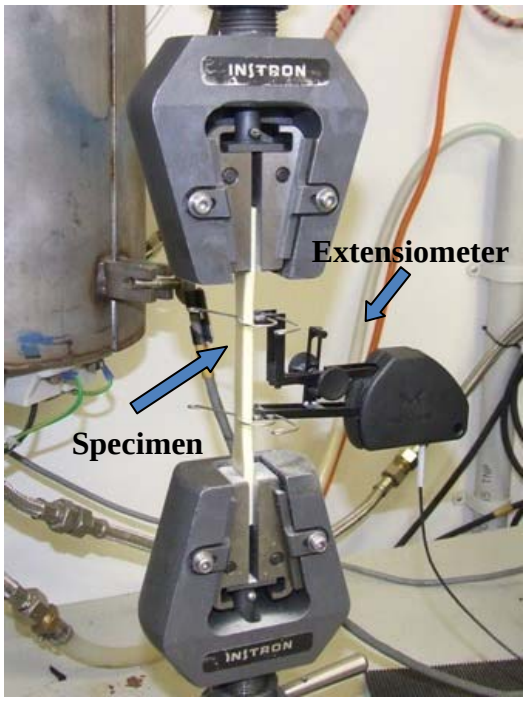

Figure 3.8: Tensile specimen in test grips

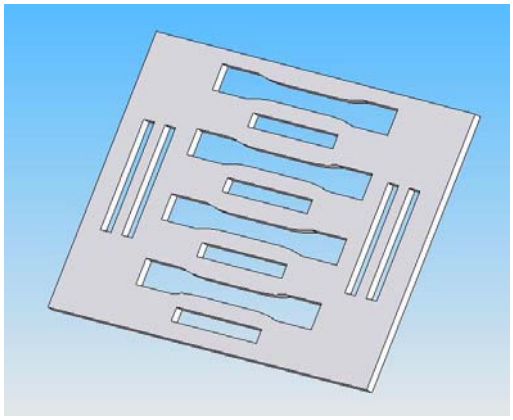

Figure 3.9: Foam cutting plan image

3.4.2. Specimens

ASTM standard 'type I' dumbbell-shaped specimens (ASTM-D638-03 [11]) were CNC (computer numerical controlled) profile cut from 293x200x6mm foam sheets (dimensions are approximate, as the mould size varied slightly due to compression and slight mould surface flexure). Specimen cutting was performed by Sign Shack Signwriters (Tauranga, New Zealand), using a 3mm router bit. Specimens were cut parallel to the length of the sheet (parallel to the foam rise direction), and were conditioned for 40 hours at 23°C and 50% relative humidity. At least 8 tensile specimens of each foam type were tested. Figure 1.5 shows the foam sheet with holes for where the samples were cut from. The larger specimens are tensile, and they measure 165mm long, 19mm wide at the ends, 13mm wide in the gauge length, which is 57mm long and curves out to the wider ends at a radius of curvature of 76mm. The smaller rectangles shown on the same image are impact specimens (80x10mm).

When the foam samples were produced, unavoidable variations in density occurred from losses during processing, so each foam sheet required post-production density calculation, to normalise the density differences between specimens. This was achieved by measuring (with digital vernier callipers) multiple specimens from each foam sheet (at multiple points in each dimension of the specimen, then taking averages) and weighing each specimen (measured to 0.001g). The weight of each specimen was divided by its calculated volume to give the individual specimen density. The specimen densities from each sheet were averaged. Similar sheets (same density and fibre type) were averaged also, then the overall average density was used to calculate an adjustment figure to normalise the mechanical performance data. This was done by dividing the normalised density by the calculated density. For example, to normalise the tensile strength result of a foam to 300kg/m^3 which was determined experimentally to be 350kg/m^3, the strength would be multiplied by 300/350, to give a reported value 0.857 times the experimental value. This linear scaling of values assumes the mechanical properties are approximately proportional to their density, as described in the Literature Review Chapter. Foam specimen types with fibre reinforcement required an additional adjustment factor to calculate the

correct foam density, rather than the composite density which is what is physically being measured. This was achieved using the known glass fibre density (2580kg/m^3) and weight fraction (5%).

3.5. Creep Testing

3.5.1. Equipment

Equipment for creep testing was not available, so a temperature controlled creep chamber was made. An old chest freezer was chosen as the basis for the creep chamber. The insulated walls and lid of the freezer were ideal for a heated creep chamber for polymer testing. Re-using it in this way is an environmentally friendly alternative to it being disposed of in a landfill. It was obtained free of charge from a local refuse station.

A specimen size of 63.5 x 12.7 x 3.18mm (from ASTM standard D2990-01 [12]) was chosen, and a rack was built with specimen supports are spaced 50mm apart (centre to centre), for up to 24 samples. 10mm diameter steel rod was used for specimen supports and the loading noses. Sheets of low density foam were placed in the base of the creep chamber to absorb impacts from weights falling due to specimen failure. This prevented shock-loading of creep specimens still undergoing testing. A small electric fan heater installed in the base of the creep chamber provided heat, and was controlled by a Yamatake-Honeywell ‘SDC20 Electronic Temperature Controller’. A thermometer/hygrometer was used to show the temperature and humidity inside the creep chamber. The separation distance of the loading noses on the stirrups was one third of the support span, shown schematically in figure 3.10, below.

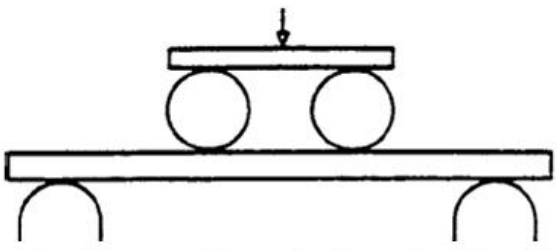

Figure 0.10: Diagram of one third support span four-point loading [13]

A device to measure the deflection of the creep samples was designed to accurately measure creep deflection, with a body which located on one side of the creep supports and rested flat on the other. This was to allow for any minute difference in creep specimen supports separation, to give consistent measurements. A Mitutoyo digital dial gauge was used in the measuring device, and measured to an accuracy of 0.001mm. A cross-section diagram of the creep specimen, stirrup and measuring device is shown in Figure 3.11. The stirrups were designed to locate between the two specimen support rods so that the loading noses were parallel with the specimen supports, and were aligned centrally on the length of the specimen. The deflection of preliminary test specimens with three point loading mode stirrups was measured on the top of the stirrup (as stirrup deflection is consistent with the specimen deflection in three-point loading mode).

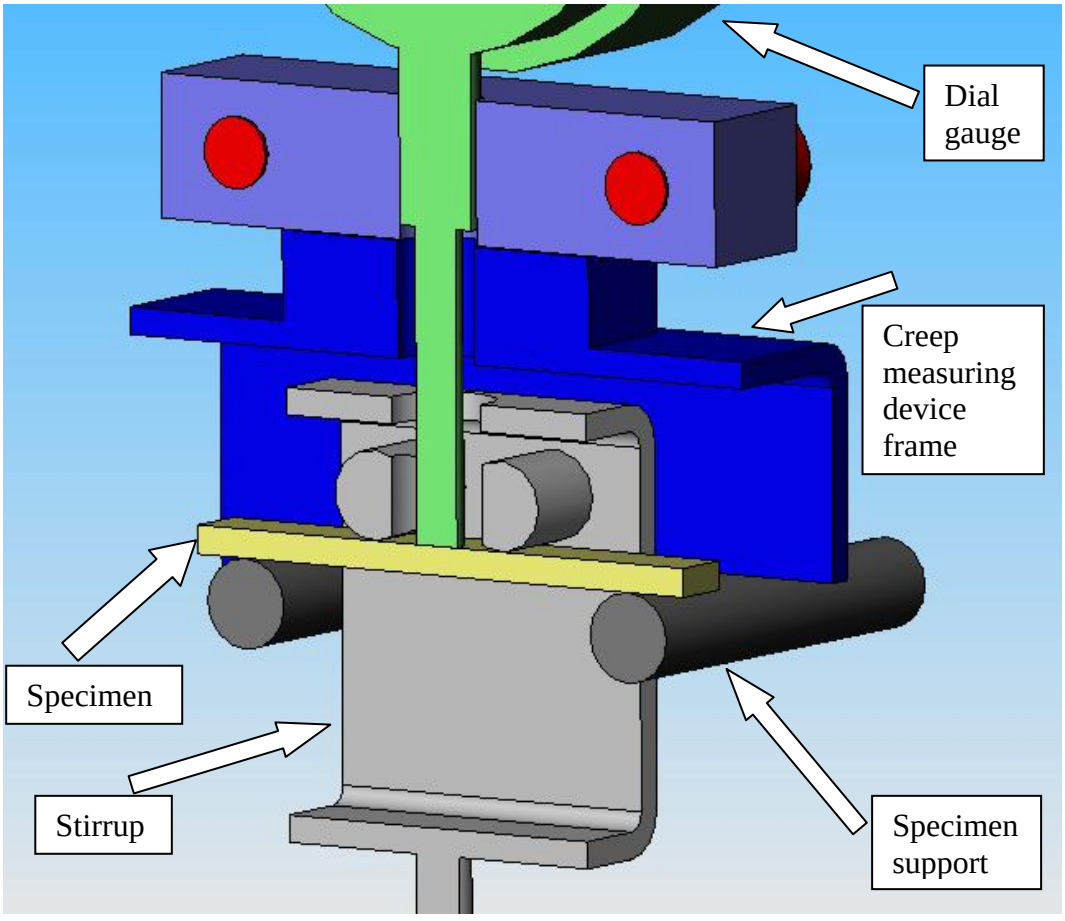

Figure 3.11: Creep measuring equipment cross-section

Weights were manufactured to be attached to the stirrups, to induce the required stress in the creep specimens. The weights were made from sections of 50mm diameter steel bar, and were drilled and tapped for connection to the stirrups with threaded rods. Various size weights were combined to make up to near the desired total weight then M6 bolts and various thickness washers were added to increase each stirrup to within 0.5 grams of the desired weight. This allowed almost any weight (within a reasonable range) to be attained.

3.5.2. Preliminary Creep Testing

Preliminary creep testing was done to first find the stress for 1% strain at 1000 hours (section 10.1.3, ASTM D2990-01 [12]). Creep testing was undertaken at 50°C. Preliminary creep testing was performed with specimens in three-point loading mode. 3.18x12.7x63.5mm test specimens were cut from 230x110x26mm foam samples, using a circular saw. All specimens were cut in the lengthwise direction of the foam sample (parallel to the foam rise direction). 5 stress levels were tested (between 2-10MPa), with 2 foam samples per stress level (one 300kg/m^3 and one 600kg/m^3 neat foam specimen). Samples were conditioned for 40 hours at 23°C and 50% relative humidity. The specimens were measured at the standard-specified times (Section 11.5, ASTM D2990-01 [12]) of 1, 6, 12, and 30 minutes, 1, 2, 5, 20, 50, 100, 200, 500, 700, and 1000 hours.

3.5.3. Phase Two Creep Testing

The change from 3 point loading to 4 point loading was for two reasons. The preliminary creep trials with 3 point loading exceeded the 5% strain limit suggested by ASTM D790, and also the results from four point loading are more meaningful, as there is a constant bending moment between the inner supports and a constant stress. Therefore creep strain versus time can be plotted rather than deflection with time [14]. The creep chamber temperature was 50°C, although for the first two hours of the test, the samples were exposed to ambient (20°C) temperature due to the number of deflection readings which had to be recorded,

and the consequent loss of heat from the chamber. The relative humidity of the creep chamber was not controlled, but was monitored. The specimens were measured at the standard-specified times (section 11.5, ASTM D2990-01) of 1, 6, 12, and 30 minutes, 1, 2, 5, 20, 50, 100, 200, 500, 700, and 1000 hours. Creep specimens cut transverse and longitudinal to the foam rise direction were tested, each at two stress levels, for each of the 6 foam types (300kg/m^3 neat, ME1020 5wt% reinforced, 101C 5wt% reinforced, and 600kg/m^3 neat, ME1020 5wt% reinforced, 101C 5wt% reinforced). Samples were conditioned for 40 hours at 23°C and 50% relative humidity. For calculation of strain (in the outer fibre of a flexural test specimen), equation 6, below, was used (where r = maximum strain, mm/mm, D = mid span deflection, d = specimen depth, L = support span. Formula from ASTM D6272 [13]).

$$r = 4.7 \times D \times d / L^2 \qquad \text{(equation 6)}$$

3.5.4. Specimens

230x110x26mm foam samples were cut into 63x12.7x3.2mm creep test specimens. The following machining and cutting methods were used to produce these:

1. The foam blocks were clamped with a large vice and the two large faces were machined flat and parallel, and the block was reduced to a thickness of 18mm.
2. The block was cut in half through the centre in the width-wise direction, and each half used for either longitudinal/transverse specimens.
3. The (injection-end) half of the foam sample was to be used to prepare longitudinal samples and the other half of the foam was used for specimens cut transverse from the foam rise direction.
4. The blocks were cut into 3.2mm slices, in the required directions,
5. The slices were cut down to 12.7mm width,

3.6. Impact Testing

3.6.1. Equipment

Notches were cut with a GBC Scientific New Zealand Notch Cutter, at a cutter rotation speed of 1400rpm. The widths at the notched zone were measured with a special notch measuring tool (which features a dial gauge and a notch locating point), as shown in Figure 3.11. The other specimen dimensions were measured with Kincrome digital vernier callipers. Specimen weights were measured with scales accurate to 0.001g.

The impact tester used was a 'Pendulum Inpact System, Model RR/IMT, produced by RAN-RAN Test Equipment LTD (Figures 3.13 and 3.14). A 0.475kg weight anvil was fitted, giving a 2.9ms^{-1} impact speed and an impact energy level of 2.0 Joules. The test span of the specimen supports was 62mm.

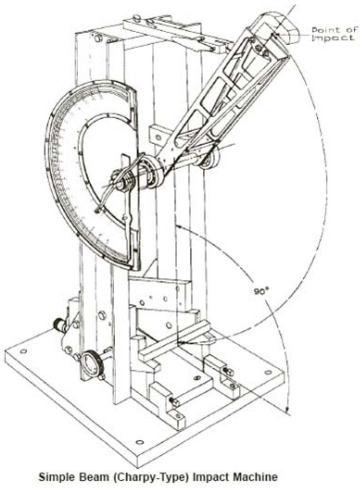

Figure 3.12: Impact Test Machine Diagram [15]

Figure 3.13: Impact tester

Figure 3.14: Impact tester anvil close-up

3.6.2. Specimens

Test specimens were CNC (computer numerical controlled) profile cut by Sign Shack signwriters, Tauranga (NZ) using a 3mm router bit, from foam sheets 293x200x6mm in size (dimensions are approximate, as the mould size varied slightly due to compression and slight mould surface flexure). Specimens were 'type 1' (ISO 179), 80mm long, 10mm wide, and the thickness was the moulded sheet thickness. Specimens were tested in the edgewise direction. 'Type A' (ISO 179) notches were cut in the specimens, with a base radius of 0.25mm, and 8mm of material remaining between the notch tip and the other side of the specimen. 6 specimens from each foam sheet were tested, 3 specimens parallel to the foam rise direction and 3 specimens perpendicular to the rise direction. Notched charpy impact testing was undertaken using ISO 179 standard methods. Specimens were conditioned for over 40 hours at 23°C at 50% relative humidity and testing was undertaken at 22° C and 55% relative humidity. Individual specimen dimensions and weights were used with to calculate specimen densities (density = weight/volume).

3.7. Interfacial Shear Testing

It was found that the interfacial shear strength between a rotomoulded PE skin and RIM PU foam filling was negligible, so standard specimens and methods could not be used. Large areas of contact were trialled, but also found to have negligible interfacial strength. A unique testing system was devised and built to test the skin/foam interfacial shear strength, which is described in Section 3.7.1.

Plain rotomoulded cuboids were produced and foam filled, as well as rotomoulded cuboids which had secondary particles added to the polymer charge. Various particles and chopped glass fibres were tested in the rotomoulding process, to assess which types migrate successfully to the centre surface of the part. The second criteria was to analyse which had an abrasive or rough surface for which the foam could successfully key into. The secondary phase particles were added to the rotomoulding polymer charge before moulding, as a single charge system (as

opposed to adding them later in the moulding, in a more time consuming double charge system).

Preliminary analysis of the above two factors was performed by visual inspection of the rotomoulded cuboids. The results of which determined the particle types to proceed to shear testing with.

3.7.1. Equipment

The rotomoulded and foam-filled cuboids were sliced transversely into five parts along the length of the cuboids, and the three central parts were used as test specimens. To test the shear strength of the PE/PU interface, a custom shear test jig was made. Figure 3.15 (below) shows the workings of the interfacial shear test jig. A specimen with a hole drilled through the centre of the foam is placed in the jig (with the pull out mechanism in place), then 5mm holes are drilled in the rotomoulded skin, where the M6 bolts (2 per side) self-tap into, to secure the specimen. The bolt-to-skin detail is shown in Figure 3.15 (note: the bolt thread is not shown in these images). The jig is clamped into a universal test machine and when tension is applied the foam pull out mechanism (shown in Figure 3.15) removes the foam from the surrounding rotomoulded skin, as shown in Figure 3.17.

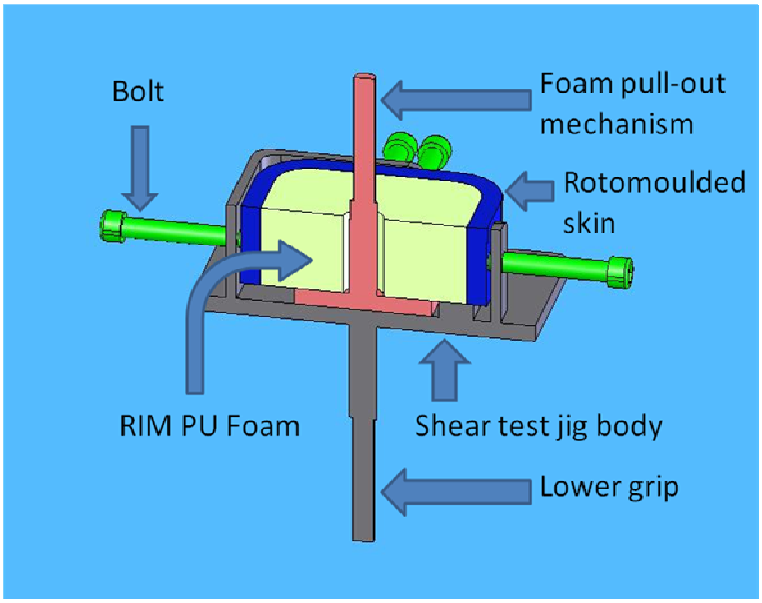

Figure 3.15: Interfacial shear test jig cross section diagram

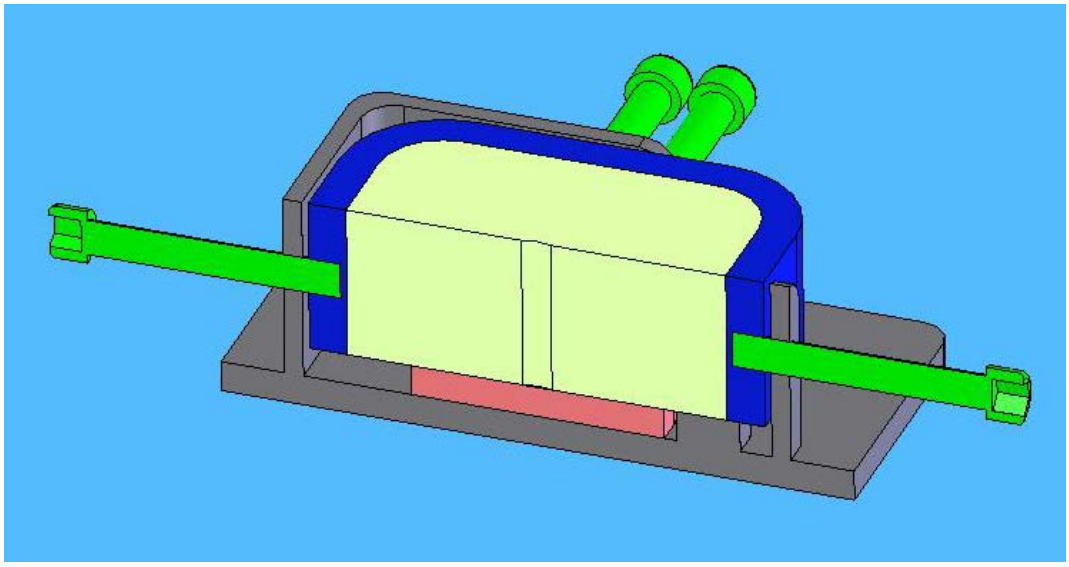

Figure 3.16: Cross section showing bolt-to-skin detail

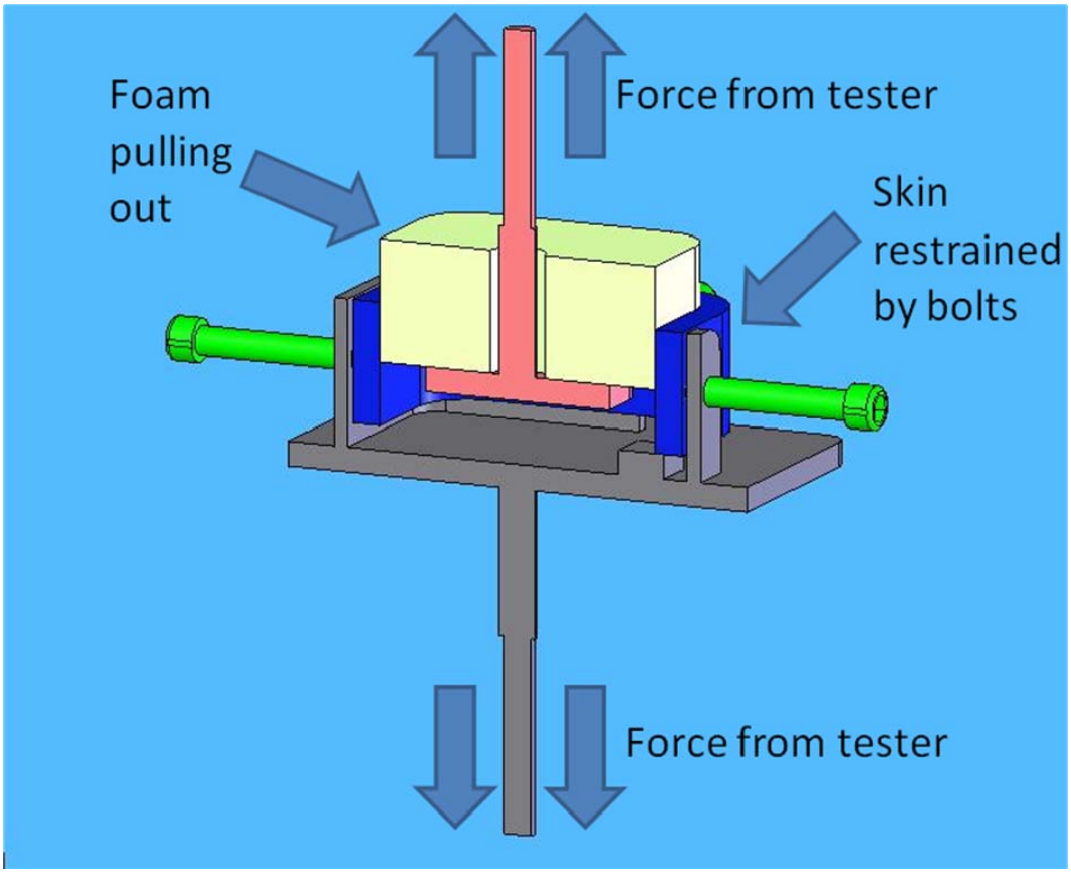

Figure 3.17: Diagram of interfacial shear test jig cross section during testing

3.7.2. Specimens

PE cuboids were processed in a small-scale rotomoulding 'R&D oven'. The internal mould dimensions were 133mm x 65mm x 65mm, and the polymer powder charge was 180 grams for all samples. The cuboids were processed to a maximum oven temperature of 190 °C, for a target internal mould temperature of 215-220°C.

Various sizes and/or types of particles (powder, sand, glass beads, powder and fibre, and steel grit and shot) were trialled as an additive to the rotomoulding charge. Each particle type were added in amounts between 1-6wt% of the polymer charge, depending on the density and/or distribution characteristics obtained from moulding. All the cuboids were made with 180 grams of Cotene 3979 rotomoulding PE.

The particles which processed most successfully were coarse aluminium oxide, coarse steel grit. Samples were produced with various weight fractions of these and test specimens cut from the foam filled cuboids as explained in Section 1.7.

Before injecting the RIM PU foam (at approximately 600kg/m^3 foam density each), the rotomoulded cuboids were pre-heated to 50-60°C (the supplier recommended foam mould temperature). A 14mm hole was drilled and an M16x2.0 thread was tapped into the top of the cuboid, which was also used to pour RIM PU foam into. The hole was blocked with a bolt when the foam had filled the cuboid and the foam had displaced the air from inside it.

3.7.3. Test Method

An Instron 4204 universal test machine (with a 5 kN load cell) was used to test the specimens, at a test speed of 5mm/min. The test was stopped when the maximum shear strength begun to decrease (after interfacial bond failure). Testing was undertaken at a 20°C and 60% relative humidity.

The shear area of the sample was determined by averaging the heights of each side of the sample and multiplying by the perimeter of the foam (once removed from the PE skin).

The maximum load was recorded from the tensile test machine, which shows the initial stress required to break the PE/PU bond. The maximum load and shear area values were used to calculate a bond-breaking load per 100 square centimetres. The results were then converted to numbers relative to the results from the specimens which had no particles added to them.

3.8. Plasma Treatment and Wettability Testing

3.8.1. Specimens

40x40x6mm square specimens of rotomoulded PE (Cotene 3979) were cut from the sides of 133x65x65mm cuboids, then air plasma treated at the Auckland University Centre for Advanced Composites Research, using a Harrick Plasma Cleaner/Sterilizer, model number PDC-32G (as seen in Figure 3.18). It has an input power of 100W, and the power applied to the RF coil for the 'High' setting used for all specimens was 18W (720V DC, 25mA DC [16]). Five specimens were plasma treated, at 1, 2, 3, 4, and 5 minutes, respectively. Chamber pressure was approximately 0.5 Torr (1 Torr = 1mmHg = 0.0193psi = 1/760 of atmospheric pressure [17]). 5 control specimens were similarly prepared but not plasma treated. In Figure 1.14 the viewing window on the top of the machine allows the RF coil to be seen, which is wound around a glass tube and has the specimen inside it.

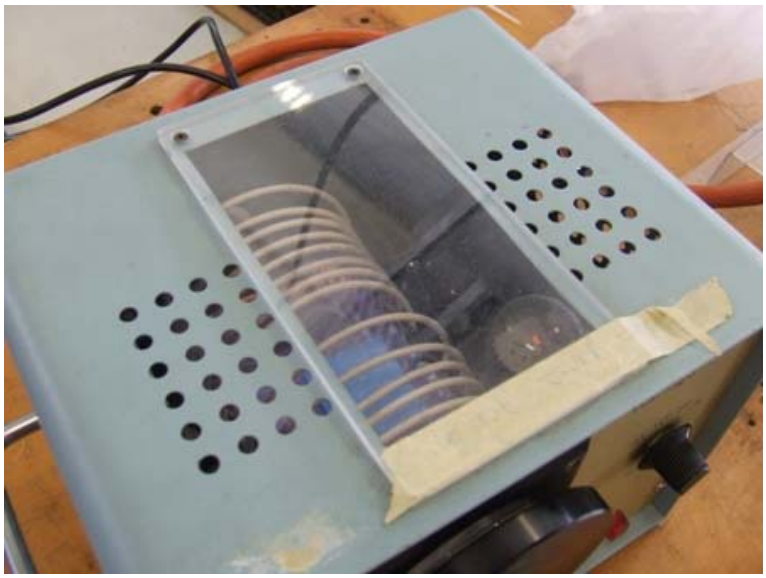

Figure 3.18: Harrick plasma equipment

3.8.2. Contact Angle Measurement

The common methods for attaining contact angle measurements include using a goniometer, or using automated contact angle measuring equipment. These apparatuses were not available, so a laboratory microscope (WILD M3B, Heerburgg Switzerland) was arranged to take side profile photographs (using a Nikon Digital Sight DS-U1) of water droplets on the specimen surfaces. 16x magnification was used to give a clear picture of the water droplet. Water contact angles were determined later by printing the images and measuring the angles with a protractor. The water used for water contact angle (wettability) testing was deionised and ultra-filtered using a 0.22 micrometer filter. This wettability testing was loosely based on the methods from ASTM D5946-04 [18]. Specimens were conditioned for over 40 hours at 23 degrees Celsius and 50% relative humidity before testing. Only three drops of water per specimen were tested, due to limited specimen size. The water droplet was applied using a syringe with a 1.05mm (outside diameter) needle, delivering approximately 3mL of water to the surface of the sample. The syringe was affixed to a vertical stand, and suspended over the specimen platform. The specimen platform was raised up for the specimen to receive the water droplet (as per ASTM D5946-04), shown schematically in Figure 3.19.

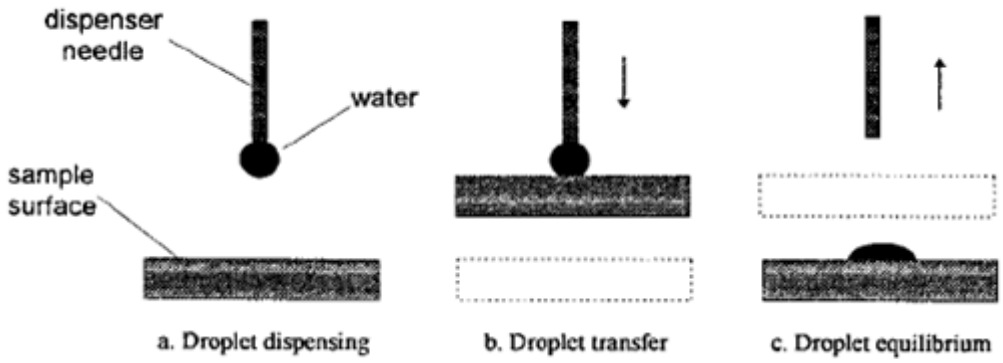

Figure 3.19: Water Droplet Transfer Technique [18]

3.9. Imaging

3.9.1. Light Box

A Kaiser 'Prolite 5000' light box was used to illuminate 293x200x6mm foam samples, and photographs were taken of the samples with a Nikon D1x camera and Nikon AF micro Nikkon 60mm 1:2.8D lens. This imaging was performed at the University of Waikato Centre for Biodiversity and Ecology Research. This method was possible because the 6mm thick RIM PU foam sheets were translucent, and due to the variation in light transmittance of the foam, glass fibre, and voids, distributions of these features were visible. The digital images were adjusted using Adobe Photoshop cs3, to show the important features more clearly.

3.9.2. X-ray

The thicker samples of foam produced (26mm thick blocks) required X-ray imaging to show fibre distributions throughout the samples produced, but voids were unable to be distinguished. The X-rays were performed by SGS (Hamilton,NZ) using a Phillips Macrotank X-ray unit. The film used was Kodak M Type 1 ultra fine grain with Pb 0.027mm back lead screen, processed manually in an Agfa G128 developer. The X-rays were photographed using the light box described in Section 1.9.1, and the digital images were adjusted using Adobe Photoshop, to show the important features more clearly.

3.9.3. Scanning Electron Microscopy (SEM)

The foam specimens were mounted on specimen platforms, sputter coated with platinum using a Hitachi E-1030 Sputter Coater, and then examined using a Hitachi S-4700 Scanning Electron Microscope at between 45x and 2000x magnification. The specimen surfaces examined were all failed tensile test fracture surfaces, of the following foams and composite foams (The fibre types are described in Section 3.2.2, and the foam densities above are approximate values):

- 300kg/m^3 neat foam,
- 600kg/m^3 neat foam,
- 300kg/m^3 foam with 5wt% ME1020 glass fibre,
- 600kg/m^3 foam with 5wt% ME1020 glass fibre,
- 300kg/m^3 foam with 5wt% 101C glass fibre,
- 600kg/m^3 foam with 5wt% 101C glass fibre,

3.10. Experimental Design Bibliography

1. *Wikipedia*. [cited; Available from: www.wikipedia.org.
2. *BOC Gases (Mount Maunganui, NZ)*.
3. *Baxenden Chemicals Limited*. [cited; Available from: www.baxchem.co.uk.
4. Haworth, H., *Baxenden Chemicals Limited*. 2006.
5. Redfern, T., *Market Technical Leader Owens Corning Asia Pacific*.
6. *Aurora Glass Fibre (NZ) Limited*.
7. *Fibreglast Developments Corporation*. [cited; Available from: www.fibreglast.com.
8. *The Fibreglass Shop (Hamilton, NZ)*.
9. *ICO Polymers (Auckland, NZ)*. [cited; Available from: www.cotene.com.
10. Betschart, P., *Abrasion Resistance of Rotomoulded Materials*. 2006, University of Waikato.
11. *D 638 - 03. Standard Test Method for Tensile Properties of Plastics.* ASTM International.
12. *D 2990 - 01. Standard Test Methods for Tensile, Compressive, and Flextural Creep and Creep-Rupture of Plastics.* ASTM International.
13. *D 6272 - 02. Standard Test Method for Flexural Properties of Unreinforced and Reinforced Plastics and Electrical Insulating Materials by Four-Point Bending.* ASTM International.
14. Gabbitas, B., *University of Waikato, NZ*.
15. *D 6110 - 04. Standard Test Method for Determining the Charpy Impact Resistance of Notched Specimens of Plastics.* ASTM International.
16. Harrick Plasma [cited; Available from: www.harrickplasma.com.
17. *Lenntech website*. [cited; Available from: www.lenntech.com.
18. *D 5946 - 04. Standard Test Method for Corona-Treated Films Using Water Contact Angle Measurements.* ASTM International.

Chapter 4 – Results and Discussion

4.1 Tensile Test Results and Discussion

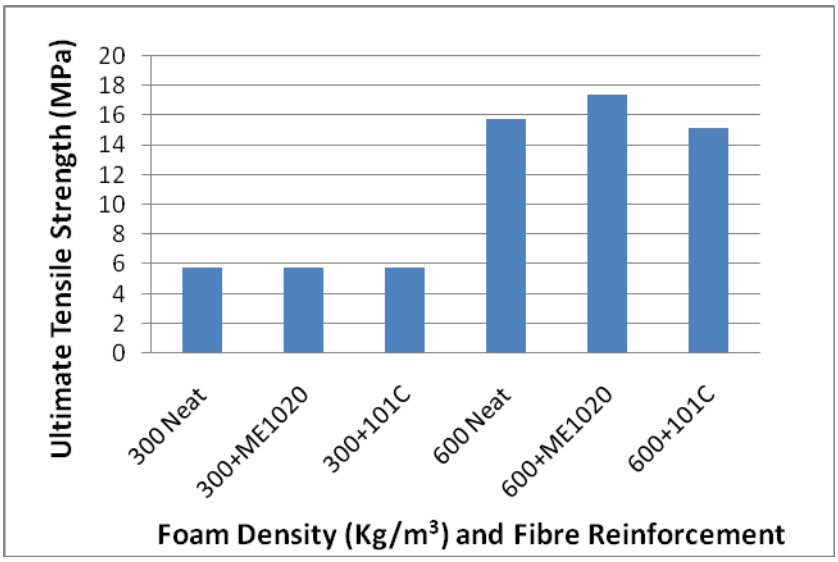

Figure 4.1: Foam tensile strength graph (specimen nomenclature explained below)

The foam specimen types in the graph are named by their density (in kg/m^3) and the fibre type (or 'neat', for non-reinforced foam). All reinforced foam tensile specimens were 5wt% fibre.

As shown in Figure 4.1, 300kg/m^3 neat foam and both types of reinforced foams are approximately the same strength, around 5.7-5.8MPa, however, the ME1020 fibre reinforced 600kg/m^3 foam results show a strength increase of over 10% above the neat 600kg/m^3 foam (17.4 and 15.8MPa, respectively). The 101C fibre reinforced 600kg/m^3 foam's strength (15.1MPa) is 4% lower than that of the neat foam. The foam properties were expected to be relatively proportional to density; however, by doubling the density from 300 to 600kg/m^3, the strength of the neat foam increased by roughly 2.7 times, and the ME1020 reinforced foam was triple the strength of the lower density ME1020 reinforced foam.

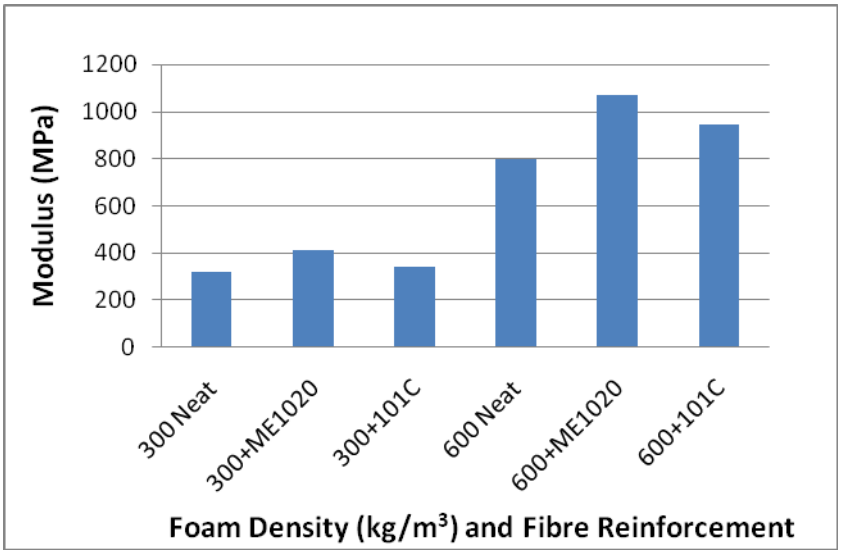

Figure 4.2: Foam tensile modulus graph

Similar (but more dramatic) trends to those witnessed in Figure 4.1, are seen in the Figure 4.2. At 300kg/m^3 density the ME1020 fibre reinforced foam displays an increase in stiffness of 29% over the same density neat foam (411.9MPa and 319.8MPa, respectively), although the 101C fibre reinforced foam has approximately the same modulus as the neat foam. The 600kg/m^3 ME1020 fibre reinforced foam displayed the highest modulus, at 1071.9MPa. This was 34% higher than the neat foam (800.0MPa) and 14% higher than the 101C fibre reinforced foam for the same density (942.46MPa). The modulus of the 600kg/m3 neat foam is 2.5 times that of the 300kg/m3 neat foam.

Due to the operation of the fibre chopper gun, some ME1020 fibres were found to be up to 2mm longer than the 6mm ideal chop length. This fibre length variation may have affected the mechanical properties of the composite foam. Also, since the exact fibre orientation distribution is not known, and tensile specimens were all tested in the foam rise direction, the degree of anisotropy is unknown.

4.2 Modelling of Tensile Properties

The Kelly-Tyson modified rule of mixtures (MROM) model (explained in Section 2.31) was used for calculating the expected strength of the reinforced foam.

Strength data from tests with neat RIM PU foam was used with glass fibre material data from literature in the following calculations.

MROM: $\sigma_c = 0.2 \times (1 - L_c/2L) V_f \sigma_f + V_m\sigma_m$

Where: L_c = 1mm, [1]

V_f = 0.0068 for 300kg/m^3 foam and = 0.0116 for 600kg/m^3 foam,

σ_f = 3450MPa, [1]

$V_m = 1 - V_f$

Neat foam strength (from experimental results:

σ_m (300kg/m^3) = 5.78MPa

σ_m (600kg/m^3) = 15.75MPa

Therefore, the strength of composite foam with 5% randomly oriented 6mm glass fibre RRIM PU strength, using above information and MROM equation:

σ_c (300kg/m^3) = 6.13MPa

σ_c (600kg/m^3) = 16.23MPa

4.2.1 Discussion

The composite foam value calculated for 300kg/m^3 is above that of the tensile strength value obtained experimentally for the suitably sized short fibre (ME1020) composite foam of the same density. The composite foam value calculated for 600kg/m^3 foam is below the tensile strength value obtained experimentally for the suitably sized short fibre (ME1020) composite foam. This could be due to the model not fitting exactly for cellular material, or possibly due to an assumption such as the critical fibre length, which was taken as the 1mm literature value for polymer composites. If this value was determined experimentally for both 300 kg/m^3 and 600kg/m^3 composite RIM PU foam, more accurate modelling may be possible.

4.3 Creep Test Results and Discussion

The specimen types in the graph keys are the density in kg/m^3, the fibre type (or 'neat' for non-reinforced), and the weight which was suspended from the sample.

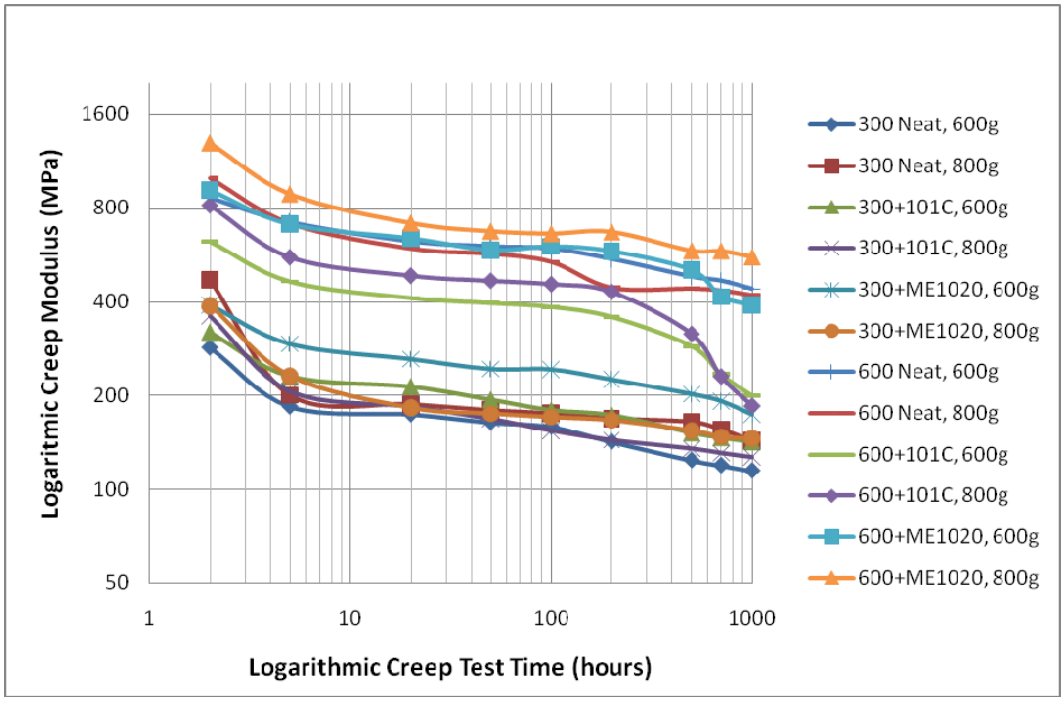

Figure 4.3: Creep modulus, 2-1000 hours

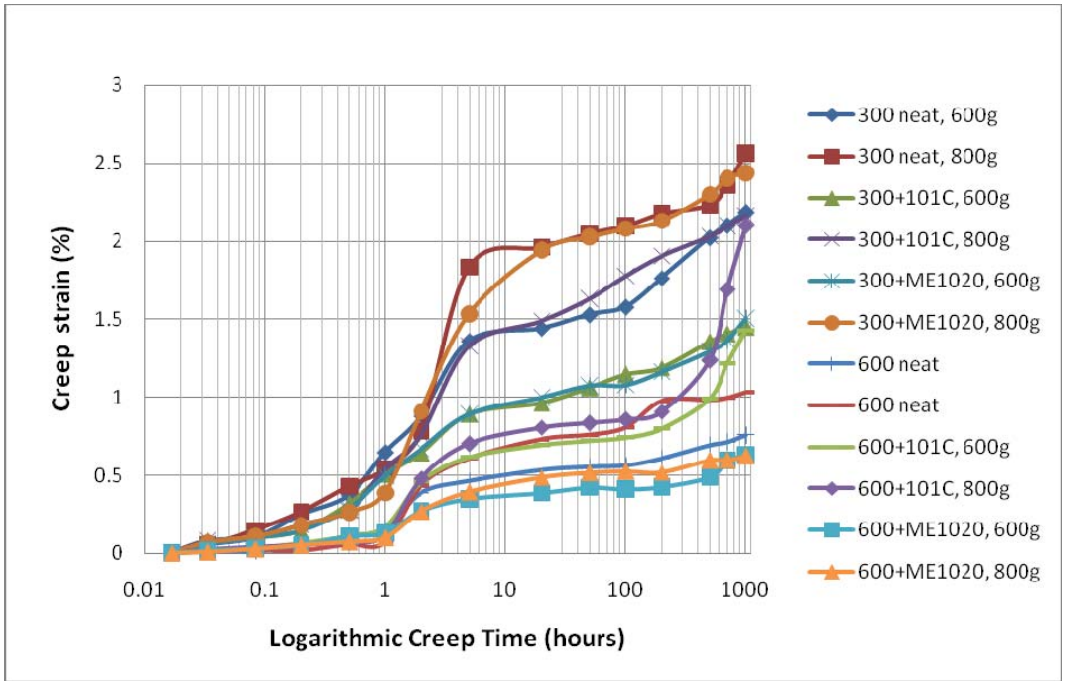

Figure 4.4: Creep strain (%) against logarithmic time

In Figure 4.3 it can be seen that the specimens approximately fall into two distinct creep modulus bands, that of the 300kg/m^3 specimens, and that of the 600kg/m^3 specimens. In the centre of these two bands are two creep modulus plots, one is 600kg/m^3 foam with 101C fibre reinforcing, which shows a lower creep modulus than the other 600kg/m^3 specimens. The other central creep plot is 300kg/m^3 ME1020 reinforced foam, which shows a higher creep modulus than the other 300kg/m^3 specimens. This indicates the ME1020 fibre reinforced foam performs better in creep than 101C reinforced foam. This is confirmed by the two highest creep modulus plots being 600kg/m^3 ME1020 reinforced foam. The neat foam specimens performed well in creep, however were seen to decrease in modulus toward the end of the 1000 hour test.

Figure 4.4 shows percent strain plotted against creep time on a logarithmic scale. This graph compares the various foam types. It can be seen that the highest creep strain values are those of the 300kg/m^3 foam specimens, which was expected due to the lower strength of these materials. In the lower portion of the graph, the specimens with minimum strains are present. The foams with the lowest creep (percent) strain values are both 600kg/m^3 specimens with ME1020 fibre reinforcement.

4.3.1 Equipment and Specimen Preparation Discussion

It was only possible to mould samples and cut into specimens so accurately, so results required adjusting to allow for different specimen dimensions or foam densities. This was achieved by calculating adjustment factors to account for variations in specimen size and density.

Problems with measurement and the repeatability resulted in some creep deflection values which were not consistent with creep (values were obtained which showed negative creep for certain time periods, which must be due to a recording or measurement error). The dial gauge recorded to 0.001mm, which is too precise for the rest of the equipment, so the measurements possibly should have only been recorded to 0.01mm. More precise equipment to match the

accuracy of the dial gauge would need to be developed for future testing, or more thorough testing undertaken so that illogical values can be easily identified and re-measured instantaneously.

Due to the calculation of creep modulus, the graph tends to infinity as the creep deformation values approach zero at the beginning of the test. This could not be plotted clearly, so creep modulus values are shown from a creep time of 2 hours onwards.

4.3.2 ASTM Discussion

When creep testing at a single temperature, the ASTM recommended minimum number of test specimens at each stress is three if four or less stress levels are used (section 8.9, ASTM D2990). This was not possible due to time and space available for creep test specimens, so only two specimens (one cut from each orientation of the foam) were tested at each of the two stress levels.

4.4 Foam/Skin Interfacial Shear Testing

4.4.1 Qualitative Analysis of Particle Additions to Rotomoulding

Most particle types trialled were found to migrate to the centre surface of the mould, except for crushed walnut shell. This became evident when it was filled with foam the foam expanded putting great force on the skin fracturing it and it consequently exploded. The weakened PE skin and high density foam effectively created a grenade type scenario. Possible reasons for the skin weakening were that the walnut shell stayed inside the thickness of the skin, essentially creating voids, and also by possible evolution of a gaseous species from the organic material, further increasing the void effect. This was not researched further as crushed walnut shell was not to be continued on with for testing.

The mechanism for particles migrating to the inner surface of a rotomoulded specimen was not determined, but thought to possibly be due to density variation between the polymer and the particle. The hypothesis proposed is that as the mould rotates and polymer sinters and becomes stuck to the walls, the heavier particles drop out of the polymer due to gravity (when at mould wall is on the upper side), then become stuck into the polymer melt again. This process would likely repeat until the polymer is in the cooing phase and the particles adhere to the inner skin sufficiently to not be removed by the force of gravity during the mould rotation. Photographs at (16x magnification) from specimens with aluminium oxide particle particles and steel particles are shown in Figures 4.5 and 4.6, respectively (the image widths are approximately 2mm). The particles are clearly exposed on the surface of the polymer and increase the surface roughness immensely.

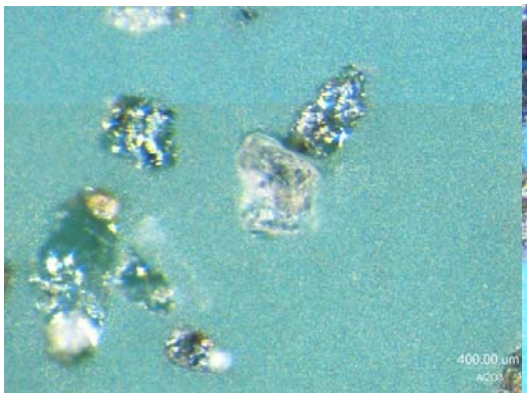

Figure 4.5: Surface with aluminium oxide

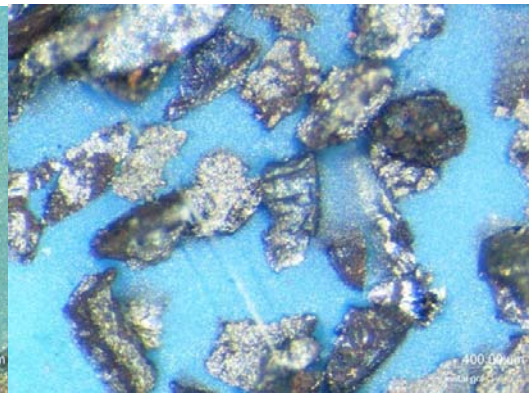

Figure 4.6: Surface with steel

4.4.2 Interfacial Shear Test Results

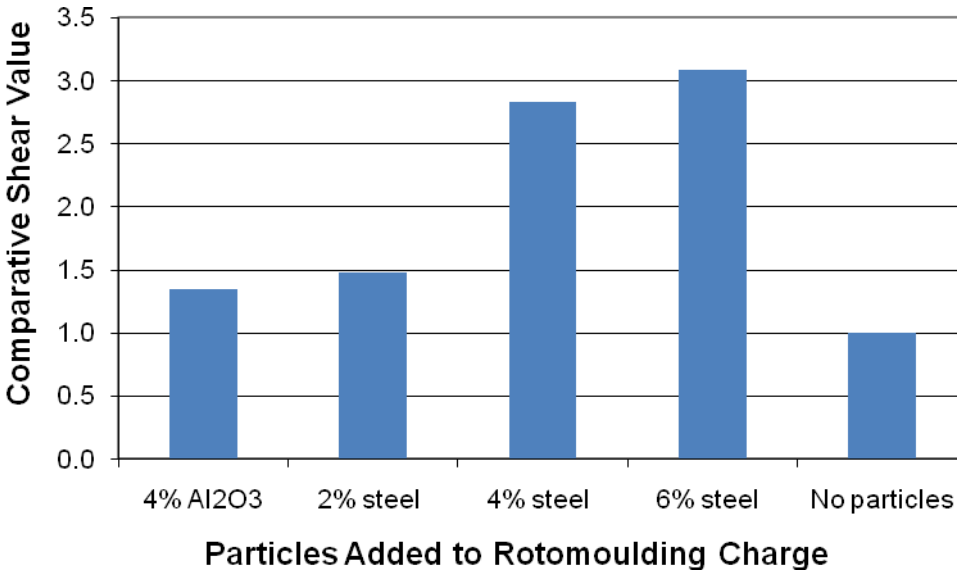

Figure 4.7: Interfacial shear test results graph (% values are weight% of rotomoulding polymer charge, 'Al_2O_3' = aluminium oxide, 'steel' = steel grit)

In Figure 4.7 the interfacial strength between the rotomoulded skin and foam filling are compared when different particles and/or weight fractions were added with the polymer charge. Due to the non-standard test method, the results are reported as a comparison against the shear strength obtained from a specimen with no particles added. It can be seen that specimens rotomoulded with steel grit showed improvement by factors of approximately 1.5, 2.8, and 3.1, for 2%, 4%, and 6% steel grit, respectively, and rotomoulded specimens with 4% aluminium oxide showed an improvement by a factor of approximately 1.3, over the 'no particles' result.

4.4.3 Interfacial Shear Test Discussion

Comparison with similar specimens which had their inner surfaces plasma treated would be an interesting test to do in the future. This would directly compare the two methods of interfacial adhesion modification.

The effect of the particles added to rotomoulded charge, on the mechanical performance of the rotomoulded skin was not assessed, so it is unknown whether or not there are any detrimental effects of this modification to the rotomoulding process.

4.5 Impact Testing Results and Discussion

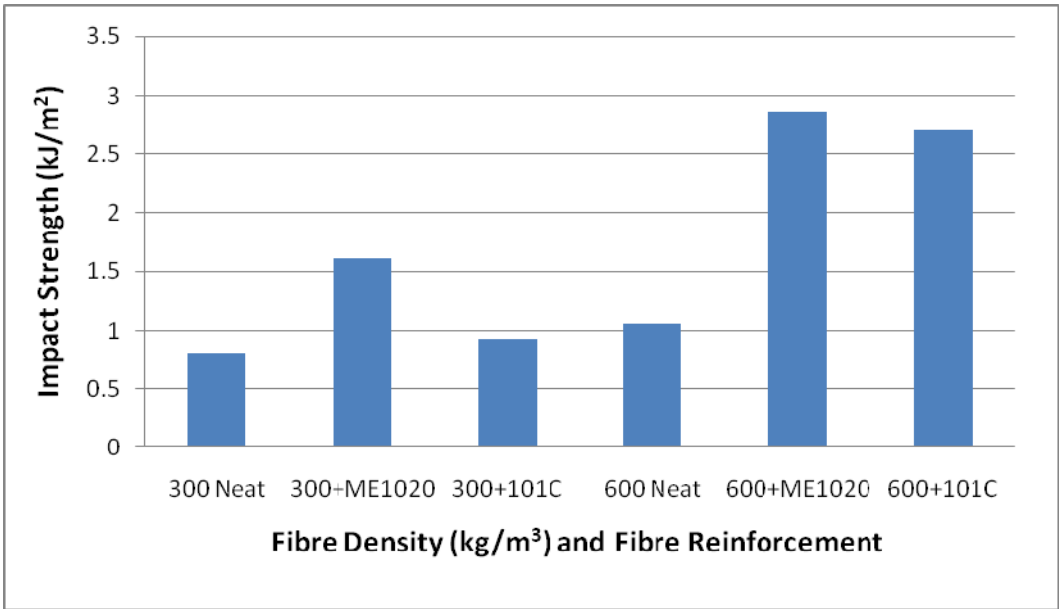

Figure 4.8: Impact test results graph ('300' or '600' refers to the normalised foam density in kg/m^3, and the letters after it are the fibre type, all 5wt%. 'Neat' means no reinforcement)

As can be seen in Figure 4.8, the impact strength of the foams tested does not show an equivalent increase for neat foam (300kg/m^3 and 600kg/m^3 results) compared to those shown by fibre reinforced samples. For both 300kg/m^3 and 600kg/m^3 samples, the ME1020 fibre reinforced specimens averaged the largest increases. 101C fibre reinforced specimens were also considerably higher impact strength than neat foam, however they were less than the ME1020 specimens, particularly for the 300kg/m^3 specimens.

4.6 Wettability Testing Results and Discussion

Examples of the images taken with the microscope are shown in Figure 4.9 and 4.10, with contact angle lines drawn on, and the overall contact angle testing results are shown in Figure 1.11.

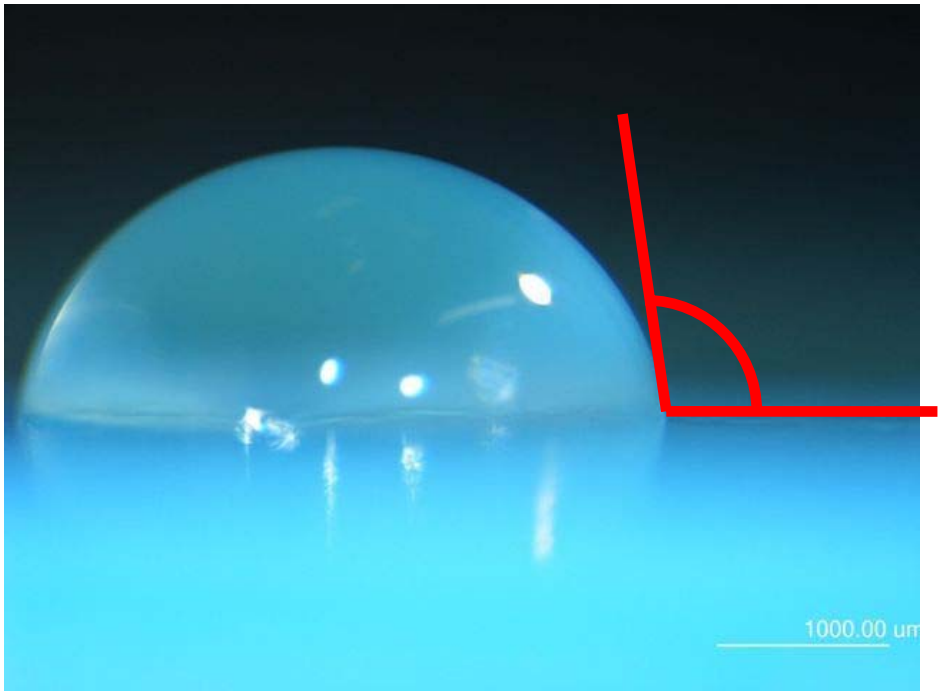

Figure 4.9: Example of non-PT water contact angle

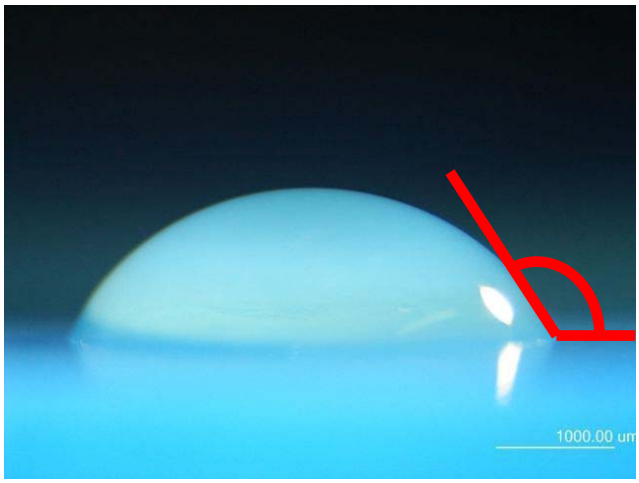

Figure 4.10: Example of air-PT water contact angle (4 minutes treatment time)

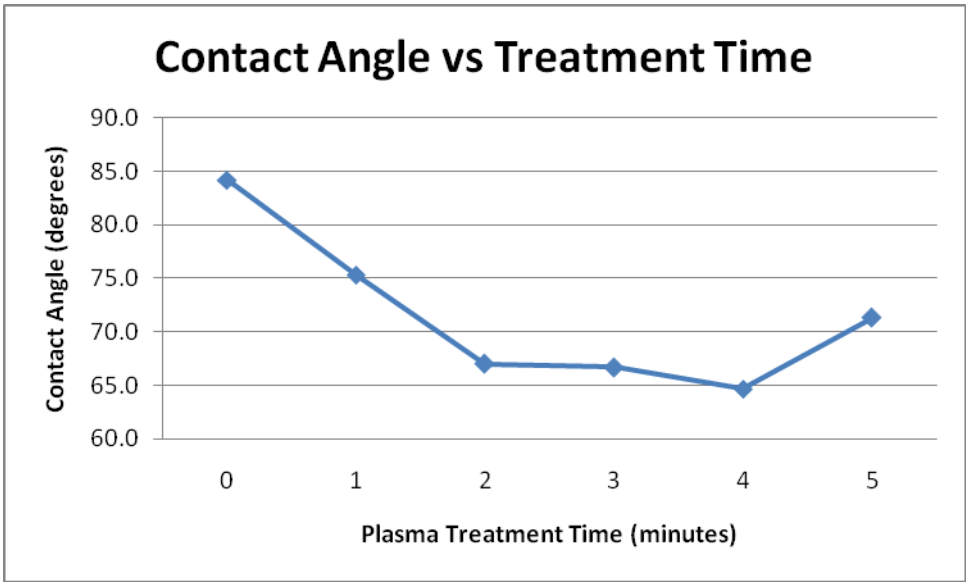

Figure 4.11: Contact angle vs treatment time graph

As can be seen in Figure 4.11, the water contact angle decreases with PT time up to four minutes, then the contact angle is larger for the five minute measurement.

This decrease in contact angle for the first four treatment times indicates increased wettability, and the higher contact angle for the five minute treatment time indicates possible overtreatment of the surface.

4.7 Imaging

4.7.1 Light Box

Two photographs from the light box imaging are shown below, with discussion of the main features present given.

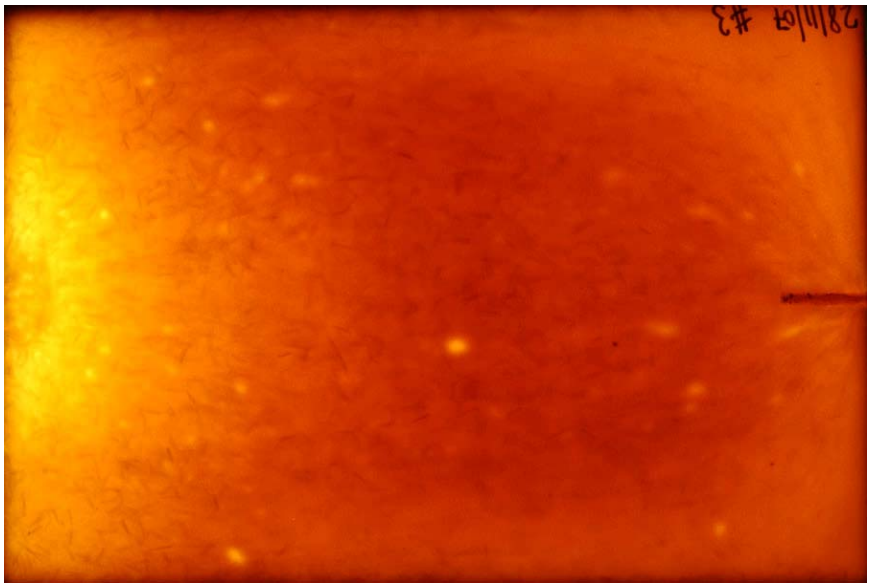

Figure 4.12: Fibre reinforced foam

Figure 4.12 shows there is a density variation over the length of the plate. The foam was injected from the plate on the right side of the image, and rose upward to the left side of the image. The flow of foam can be seen to migrate outwards from the injection point in a ‘v’, and move up the mould evenly from approximately half way along its length. At higher image quality the fibres are seen to be well distributed throughout the foam, and quite randomly oriented. The line on the right of the image is due to a mould defect (not a localised region of high density). This plate has a large void in the centre, which is visible as a lighter colour dot.

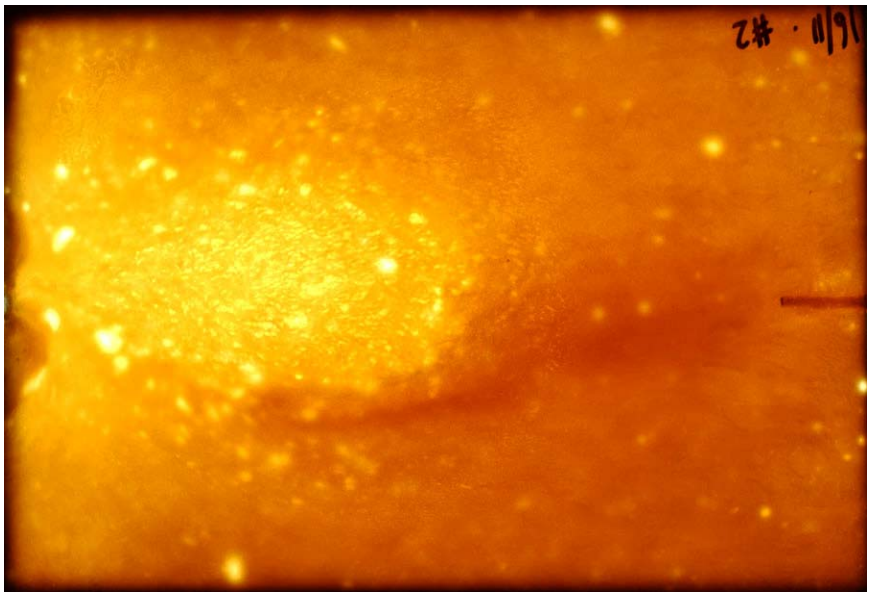

Figure 4.13: Light box image of neat foam

The sample in Figure 4.13 is a lower density (around 300kg/m^3), and has many voids. There is an uneven density variation also, which may suggest the foam components were not mixed adequately, or some other effect is occurring to cause this.

4.7.2 X-ray

Two X-ray images are shown below, and the main features are discussed. The X-rays of non-reinforced foam sampled did not give useful information, as the voids did not show. However, the X-rays were found to show the fibre distribution and orientations well. This was converse to the light box images, which showed voids clearly, but, did not show the fibre distribution as well.

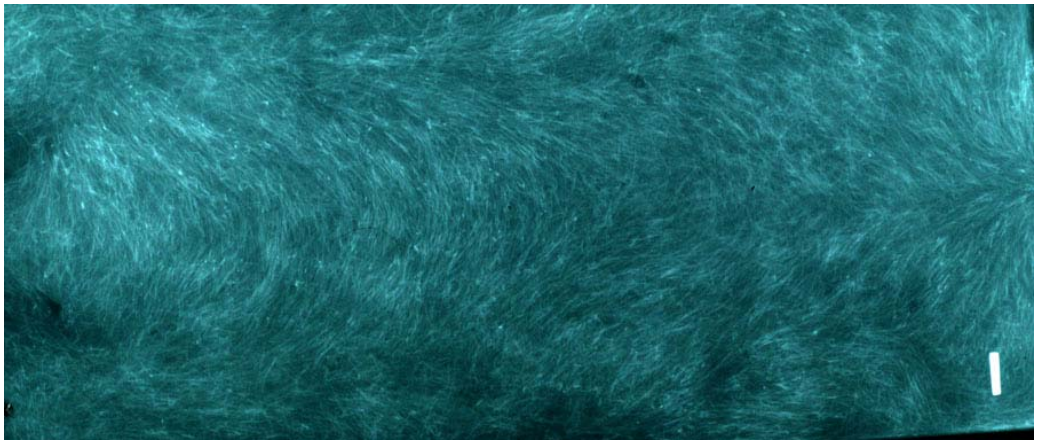

Figure 4.14: ME1020 fibre reinforced foam X-ray

Fibres are visible in Figure 4.14, which tend to align in certain patterns along the length of the specimen. The foam injection point is at the right of the image. Fibre in the centre of the injection point half of the sample tend move away from that central point in a fan pattern then from the middle up the sample, rising upwards (moving left on the image) the fibres are seen to align with the mould walls, and align perpendicular to the rise direction in the centre of the sample. On the left of the image, turbulence is seen (which is the top of the mould).

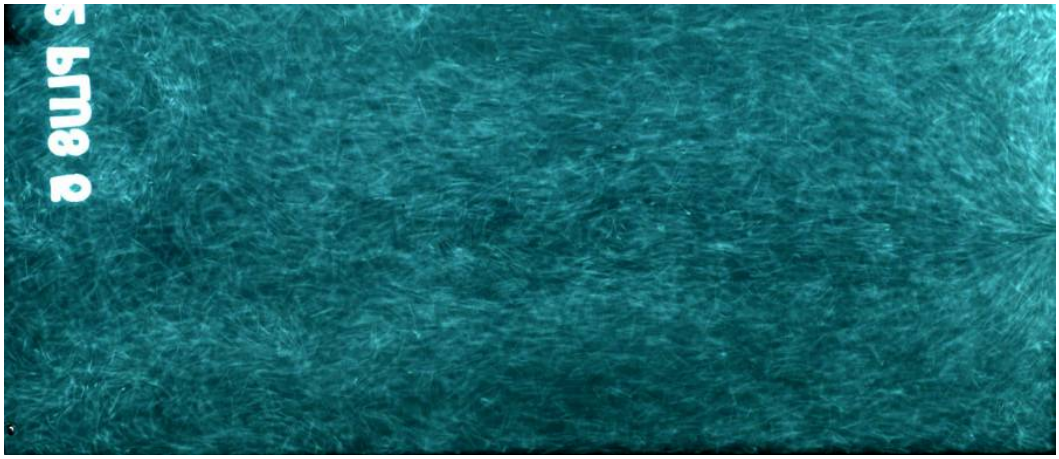

Figure 4.15: 101C fibre reinforced foam X-ray

Figure 4.15 shows similar trends to Figure 4.14, however the fibres are more aligned with the flow direction in the centre of the sample. The fibre in this sample was purchased pre-chopped and it appears that the fibre bundles remain together, as opposed to in Figure 4.14, where the fibres appear to be finer and more separated.

4.7.3 Scanning Electron Microscopy

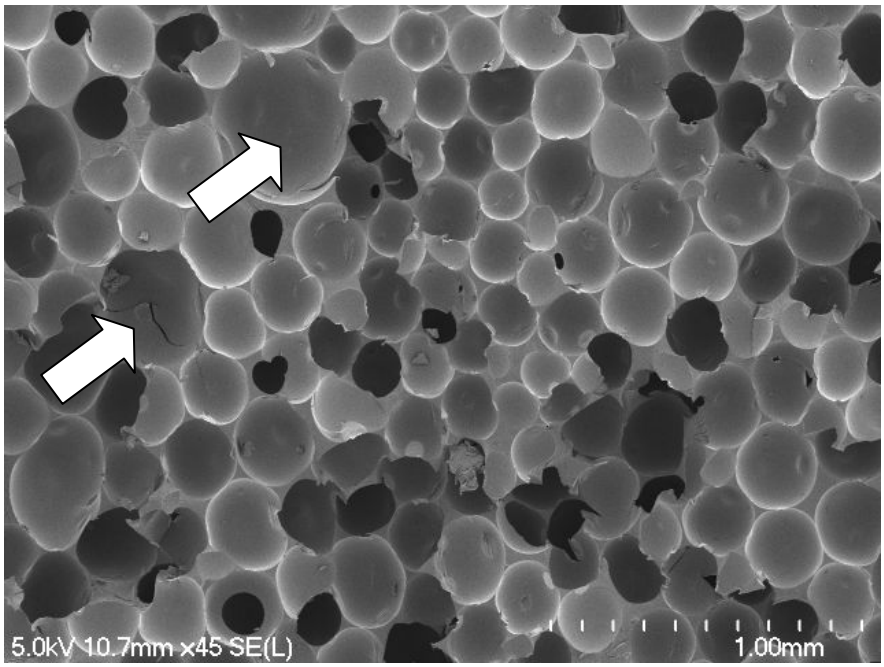

Figure 4.16: SEM image 300kg/m3 neat foam

Figure 4.16, above, shows the spherical cell morphology and the average cell size approximately 0.2mm. Some cells are larger, such as is shown by the arrows (in the upper left quadrant of the image). The circular cells visible in this image are concave, spherical gas pockets which have been fractured roughly in half. Also, the darker cells which appear to look like tunnels are merely 'shadows' and are likely to be similar size and shape to the rest of the cells. The tensile fracture surface visible here is roughly flat, which is characteristic of a brittle failure.

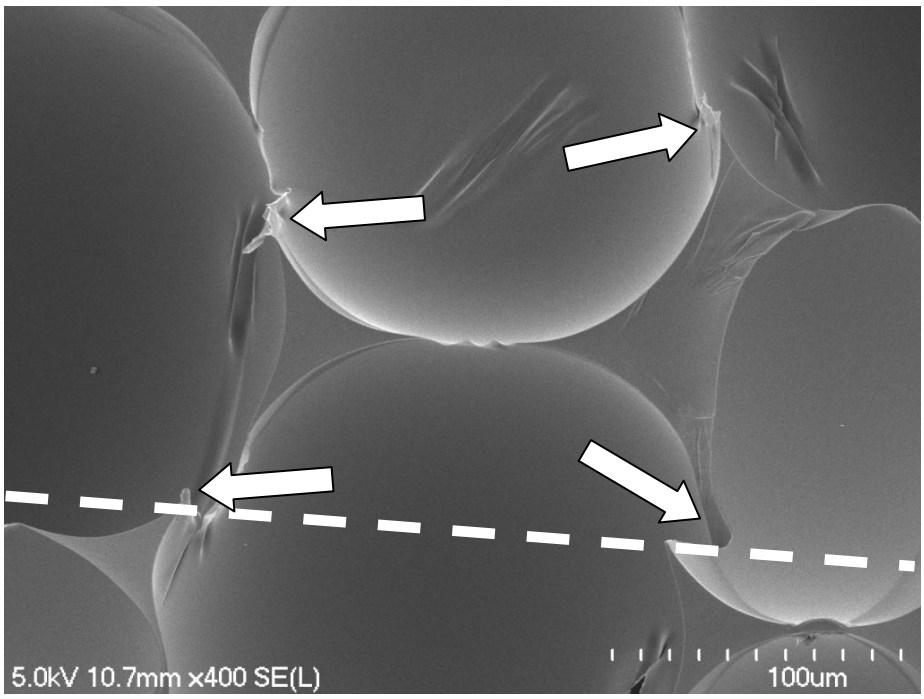

Figure 4.17: SEM image 300kg/m3 neat foam

In Figure 4.17 above, the fracture surface appears to step between cell planes, in regions of thin material between cells. The two arrows in the lower part of this image show regions where this has occurred. A dotted line has been put into the image to show the upper and lower sides of the fracture step. A similar, but smaller step is visible on both sides of the cell in the top centre of the image, shown by the top two arrows. This shows that although the macroscopic fracture surface is reasonably flat, the microscopic fracture surface propagated up and down between different cell planes, following the path of least resistance (the thinnest areas of material). The minimum wall thicknesses between cells are

approximately less than or equal to 5 µm. A wrinkled surface is visible in the cells in the top centre and top right side of the image. This is discussed later.

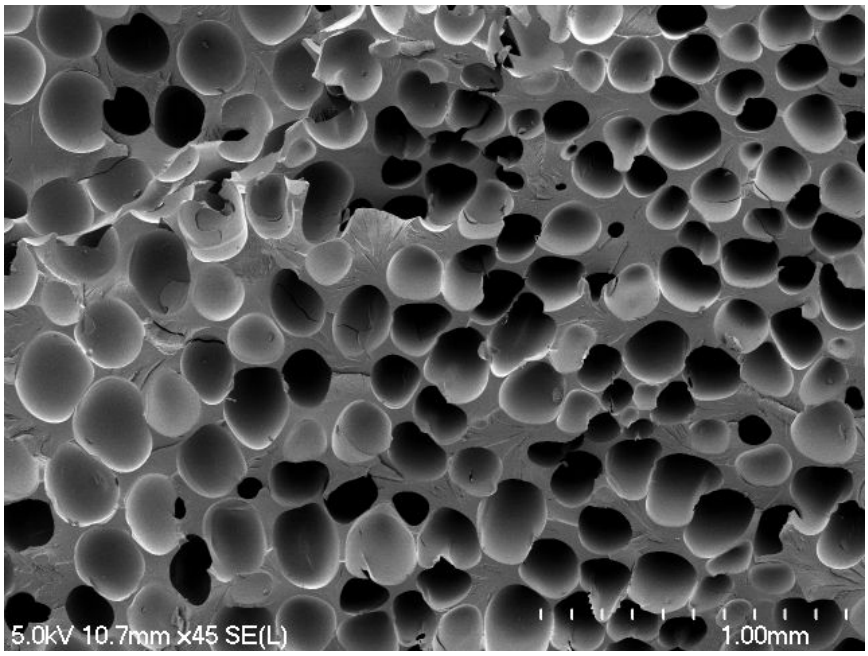

Figure 4.18: SEM image

Figure 4.18 above, shows the common cell sizes range is 0.1-0.3mm. The average minimum wall thickness between cells is visibly thicker than the 300kg/m3 foam specimens. On the left side of this image the cells are larger than the right side of the image (approximately 0.25mm cells left and approximately 0.15mm right). This shows that the foaming is non-uniform, which may possibly be due to un-uniform distribution of foaming agent.

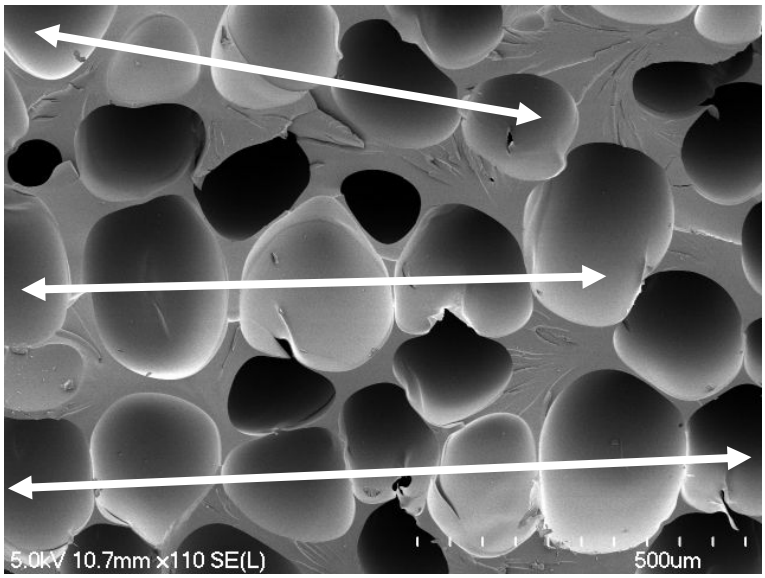

Figure 4.19: SEM image

Figure 4.19, above, shows 600kg/m3 neat foam at 110x magnification. The common cell size is approximately 200µm. Minimum wall thickness between cells (at cell point-contacts) is approximately 10 to 100µm. There appears to be 'strings' of cells which have minimal material between them and more material between 'strings'. Three series of these are highlighted in this image with long arrows. If this trend is consistent over the entire foam structure, and aligned such as these three examples are, it could possibly cause anisotropic properties (with higher strength in the direction parallel to the 'string' of cells). Anisotropy in neat foams is usually attributed to cell elongation (and commonly only present in free rise systems), but cell elongation is not present here (and this is a closed system foam).

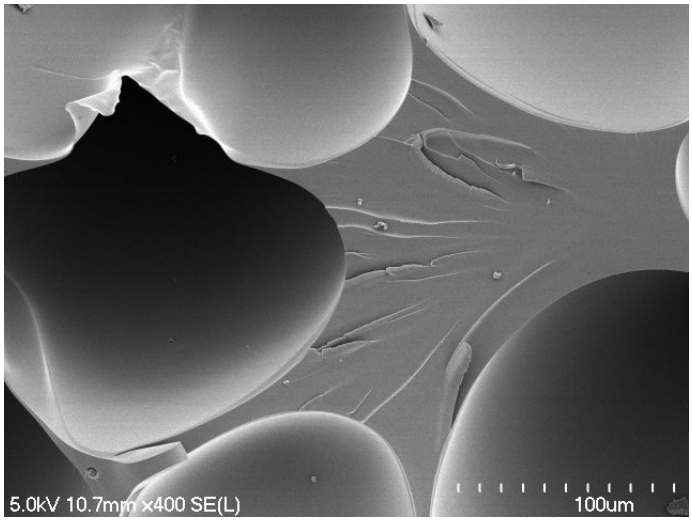

Figure 4.20: SEM image

Figure 4.20, above, shows 600kg/m3 neat foam at 400x magnification, to examine the microscopic fracture surface. The cell wall in the top left of the image has torn and was only a few micrometres thick. Another feature visible in this image is the bulk polymer material is not itself cellular. Some foamed polymers have a macrocellular structure as well as a microcellular structure, but RIM PU foam only has macrocellular structure. Although the foam specimen failure was found to be brittle, the microscopic failure mode appears to be partially ductile, with lines from shearing visible in this image.

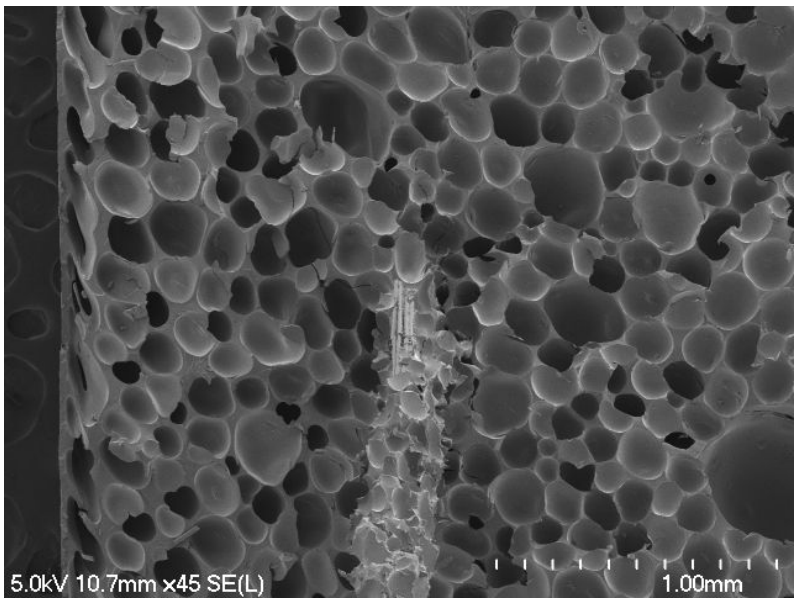

Figure 4.21: SEM image – 300kg/m3 foam with 5wt% ME1020 fibre

In the centre of Figure 4.21 is a fibre bundle which has pulled out of the other side of the fractured surface. As can be seen, polymer foam is still surrounding the bulk of the fibres. This suggests that the fibre/matrix interfacial strength of these fibres is stronger than the foam matrix itself. On the left side of the image, cell elongation is visible. This is the edge of the sample and would have been caused by friction from the foam mould wall. A 'skin' is also evident, approximately 20μm thick. This foam specimen has a large variation of cell size, and a void is present in the lower right side of the image.

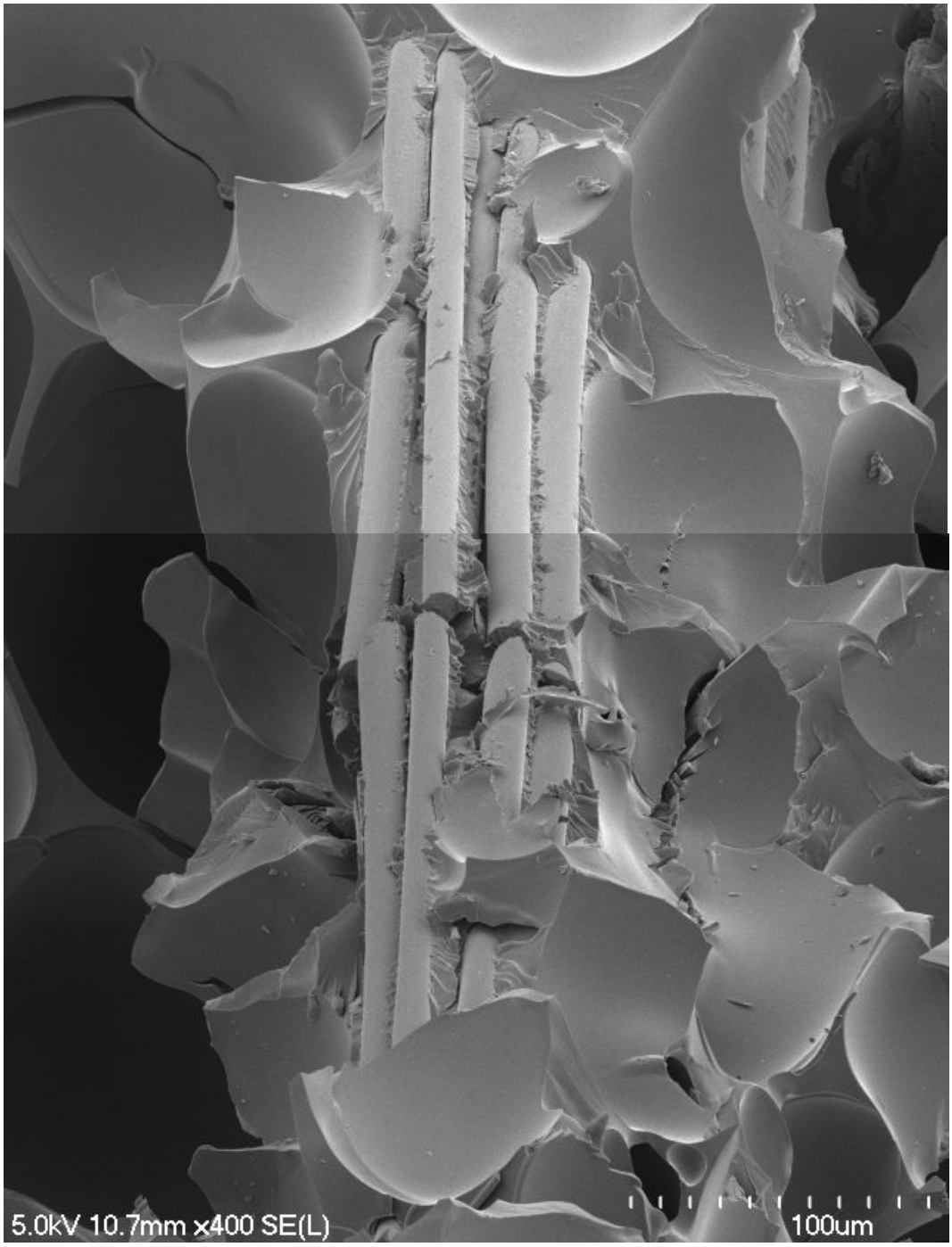

Figure 4.22: SEM image – 300kg/m3 5wt% ME1020 fibre

In Figure 4.22, above, it can be seen that the fibre bundle was fully wetted, and the cells appear to form around the fibre bundles, forming an encasing skin, The foam appears to form a skin around the fibre, much like is witnessed at the surfaces of moulds. In the centre of the image some fibre breakage is visible. Although the fibres are broken, the bundle still pulled matrix material out of the other side of the fracture surface, which suggests that there is very good load transfer between fibres the matrix.

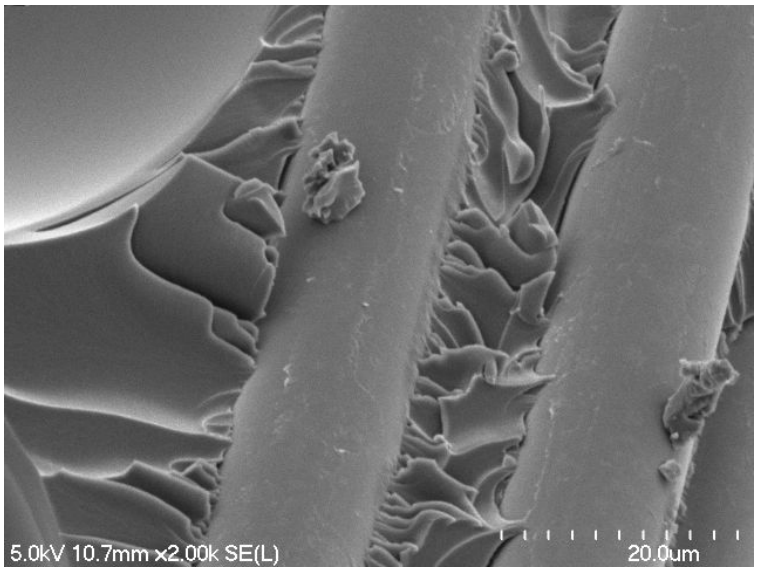

Figure 4.23: SEM image

Figure 4.23, above, shows 300kg/m3 foam with 5wt% ME1020 glass fibre, at 2,000x magnification. In this image, two glass fibres are shown, surrounded by solid PU matrix material. The corner of a cell can be seen in the top left corner of the image. The matrix fracture surface shows the microscopic fracture mode of the foam is plastic failure.

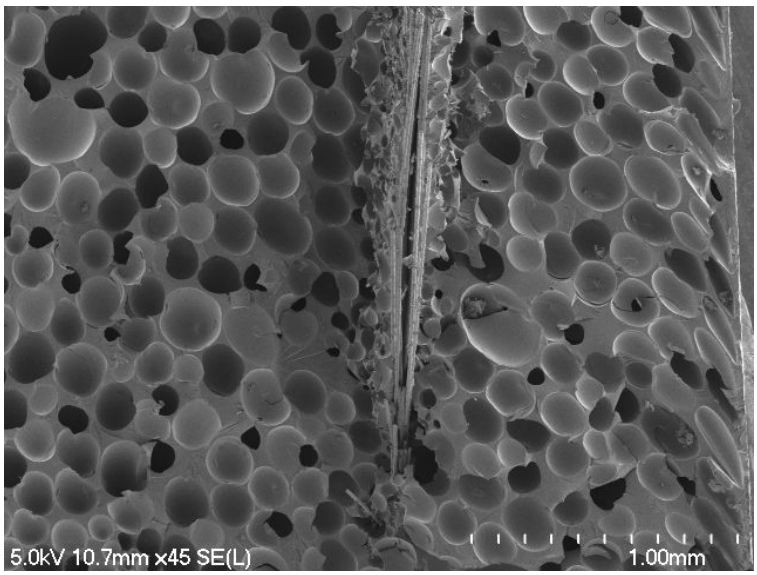

Figure 4.24: SEM image – 600kg/m3 5wt% 101C reinforced foam

In Figure 4.24, above, the fibres appear to be transverse to the loading direction, which may have been a cause of specimen failure initiation. The cell elongation

visible on the right side of the image (which is the edge of the specimen) gives an indication of the foam flow direction during moulding. The fibre bundle visible appears to be aligned with the flow direction Cell elongation is present on the right side of the image, which is at the mould surface. Here it is limited to within 0.2mm of the surface of the sample so should have little effect on the bulk properties. There is fractured foam material on the outside of the fibre bundle extending out of the fracture surface, which shows the polymer is bonding well to the fibre. However, the central region of the fibre bundle appears to not be wetted out by matrix material.

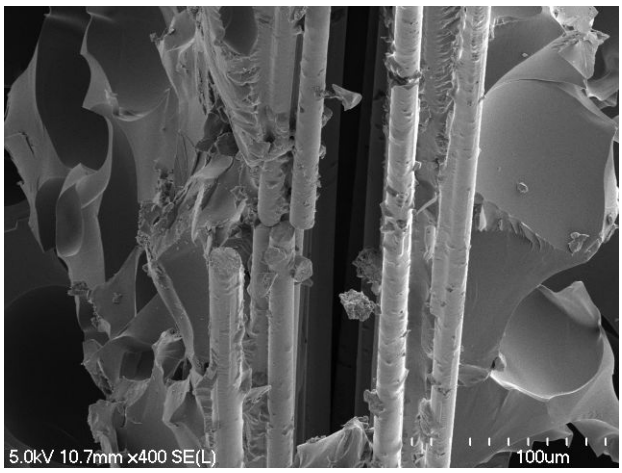

Figure 4.25: SEM image

Figure 4.25, above, shows 600kg/m^3 foam with 5wt% 101C glass fibre, at 400x magnification. This image shows the poor wetting of the middle of the fibre bundle. There appears to be matrix bonded to the fibres either side of the cavity.

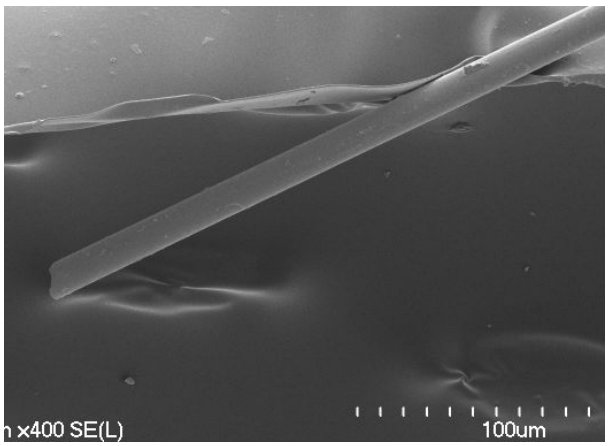

Figure 4.26: SEM lone 101C fibre

Figure 4.26, above, shows a lone fibre which has a smooth surface and does not appear to bond well with the matrix. This fibre is not sized suitably, so was not expected to bond as well as the correctly sized fibre.

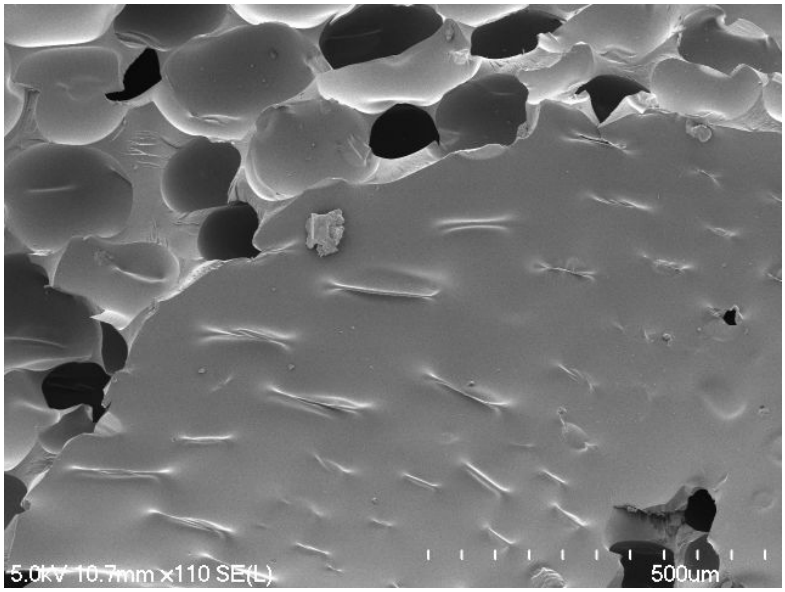

Figure 4.27: SEM image

Figure 4.27, above, shows the inner surface of a large void at 110x magnification. Many lines or wrinkles can be seen on the void surface, which required closer investigation (shown in Figure 4.28).

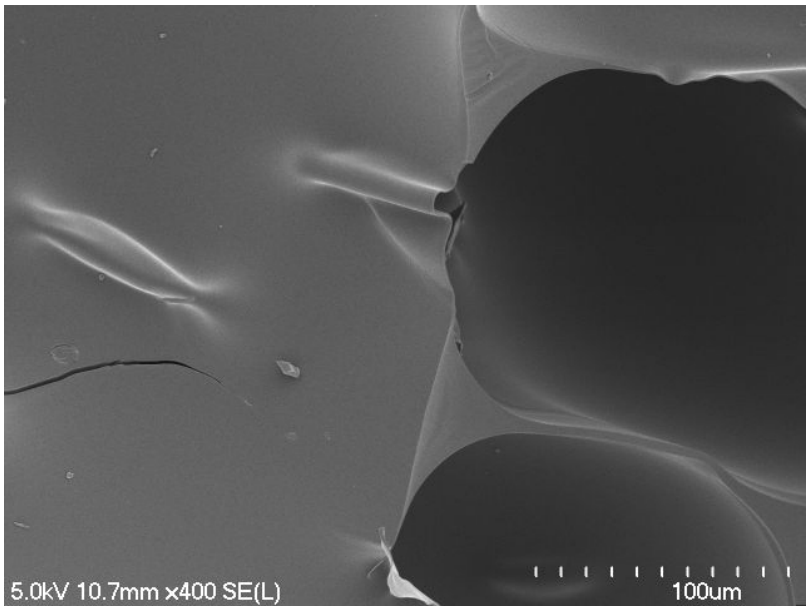

Figure 4.28: SEM image

Figure 4.28, above, shows a close up of one void surface wrinkle which has fractured through the centre to expose its cross section. It was thought the wrinkles may have been matrix-encased fibres, but this shows that it is a fold in the thinnest region of material between two adjoining cells. This is considered to possibly be due to plastic deformation of the thin part of the cell wall during tensile strain before failure. When the surrounding material elastically returned to its original dimensions after fracture and this area did not, it became a wrinkle in the void surface.

4.8 Results and Discussion Bibliography

1. Callister, W., *Materials Science and Engineering an Introduction*. 6 ed. 2003: John Wiley & Sons, Inc.

Chapter 5 – Conclusions and Recommendations

5.1 Conclusions

The mechanical properties of RIM PU foam were found to increase with, but not proportionally to, increases in density. For example, tensile strength and stiffness gave up to three-fold improvements when the foam density was doubled from 300 to 600kg/m^3, however, the impact properties only increased by a small amount when neat foam of the same densities were tested. Therefore, an overall conclusive statement about the mechanical properties of the foam relative to the density (or cost, for example) can not be provided until the parameters are highlighted that are most important to assess. This will require more depth analysis of the products being developed for which the foam is to be used with. For example, a sandwich structure analogy was presented where under bending loads, shear, compressive, and tensile properties are all important. However, if the product is in pure compression, maximising the shear and tensile properties of the foam would not be beneficial to the product.

Fibrous reinforcement of the foam with two different fibre types was researched and tested. One was suitably sized for the matrix, but required chopping to use, and the other was conveniently pre-chopped, but not suitably sized. Mechanically testing the performance of the two composite foam types shown the suitably sized fibre had similar or better properties in all cases. Due to the different chopping methods of the two fibre types, the lengths and bundling were noticeably different. Further analysis of these features would need to be undertaken before the fibre sizing is conclusively attributed to the higher performance composite properties.

Air plasma treatment was shown to give good wettability improvement of rotomoulded linear high density polyethylene (HDPE) specimens, even when tested long after the treatment was undertaken.

The addition of steel grit to the rotomoulding charge was found to successfully improve the foam/skin interfacial shear strength of a foam-filled rotomoulded product.

5.2 Recommendations

5.2.1 Full-Scale Product Testing Recommendation

Full-scale (or larger specimen size) testing is recommended to validate the test results obtained from small laboratory test specimens. Assessing bulk material samples is important firstly because standard test methods require the exclusion of specimens with obvious flaws such as voids (so will sometimes give optimistic results), and secondly because as the foam rises and reacts to form a solid material, the dispersed fibres tend to align in the foam flow directions and cause anisotropic properties. Failure to design and engineer with consideration for these two features may lead to inadequate product performance. CAD modelling/FEA of the product would also be recommended to assess the importance of the interface and to determine the stresses acting on the foam.

5.2.2 Foam/Skin Interfacial Strength Testing

It would be beneficial to test full size (product) samples which have been internally plasma treated and foam-filled, against full size samples which had particles added to the rotomoulding charge and foam-filled. This would both verify the results for shear testing that was done on smaller specimens (of cross sections of rotomoulded and foamed parts), and directly compare the performance benefits of each of these alterations to the processing method. Alternatively, plasma treated cuboids which were prepared and foam-filled similarly to the specimens with particle additions, could be shear tested by the same methodology, to directly compare the two methods. It would also be recommended to undertake a full cost analysis of the two methods for improving interfacial strength. This would show the short and long term costs. Because the plasma treatment option

has an initial equipment cost, but a low ongoing cost, and the particle addition method has no equipment cost but high ongoing cost, the point and rate at which the two cost plots cross one-another would be useful for deciding which method to use, if one was to be chosen.

There was a large (over 100 hours) time delay between PT of specimens and the water contact angle testing, therefore aging of the PT may have occurred and affected the wettability results from those which may have been obtained if they were tested immediately post-treatment. Testing the wettability at various intervals would be recommended to examine how this is affected by time for the particular treatment that is done. In manufacturing there may be large delays between PT and foam filling; therefore by testing the effects of PT aging on rotomoulded components, the importance of this can be assessed. Testing the specimens with different process gases (such as argon, nitrogen, and oxygen), power levels, and pressure levels could also be beneficial. This process may be more meaningful to manufacturing if full size products were plasma treated. The additives in rotomoulding materials to prevent oxidation during the rotomoulding processing stage may have affected the PT effectiveness. Further investigation of this would be recommended.

5.2.3 Imaging

Micro computer tomography (micro-ct) imaging of the fibre reinforced samples could be undertaken to attain 3d images of the fibre orientation and distribution. This would be important in the product due to the complex geometry which will likely create turbulence and/or fibre alignment during the foam rise stage, which can create anisotropic properties. Micro-ct could also be used to determine the fibre length distribution. This would show how much fibre breakage is occurring during foam processing.

Further investigation using SEM is recommended. Features to examine (or examine in more detail) include dry fibre bundles. The ME1020 and 101C fibres used in testing were visibly different in their bulk density and bundle sizes, so by

examination of the bundle size of fibres chopped with a chopper gun and fibres purchased pre-chopped would be beneficial. If accurate knowledge of fibre length distribution of pre-processed fibres was known, more meaningful comparisons between fibre types could be given. Examining post-processing fibre lengths may be beneficial, to determine how much fibre breakage occurs during RIM PU foam processing. This was assumed to be minimal, but if fibres are in fact becoming broken into shorter fibres during processing, this may affect product properties.

Also, the fibre surfaces could be examined, to determine whether the layer seen in 101 fibres examined was in fact a sizing layer or matrix material bonded to the fibre. The 'skinning' effect noticed in could be looked at in more detail, as well as the 'strings' of cells noticed, to determine whether they are randomly aligned, or whether some pattern or consistency is present. The effects on mechanical properties of samples taken parallel and perpendicular to these 'strings' could also be tested to determine whether or not they alter the properties. Lastly, the cause would need to be determined, such as, if the rise direction or some other factor is controlling them, these could possibly be controlled or manipulated to give advantageous properties.

5.2.4 Compression Testing

It is recommended that compressive properties be tested, as this was not possible at the time of testing.

5.2.5 Creep Testing

Due to time limitations on testing, creep was not tested longer than 1000 hours, but for ensuring long term performance, creep testing at elevated temperatures should be carried out for periods exceeding 3000 hours. Testing with the specimen numbers specified by the standard, plus specified control specimens, would give more accurate results also. This was unable to be done due to time and creep sample space limitations.

5.2.6 Surface Chemistry Analysis of Plasma Treated Specimens

It would be beneficial to do ATR-FTIR spectroscopy analysis of plasma treated rotomoulded PE to examine which surface reactions have taken place. Also examination of the surface morphology using SEM would be beneficial for analysis also.

5.2.7 Elevated Temperature Testing

Testing such as impact, tensile, and compression should be undertaken at elevated temperature (ie. 50°C), as the properties at this temperature need to be known, to ensure that in warmer climates the product/s will be able to withstand the design loads. Water contact angle testing of plasma treated samples which are/have been heated to 50-60°C would be beneficial, as this is the temp which the product will have to be heated to before injection of foam occurs. If the plasma treatment effect is diminished by heating to this temperature, then the surface treatment may have to be modified (different gas/treatment time/power level, or a different system/method).

5.2.8 Testing for Degree of Anisotropy

Tensile testing foam samples which are cut with their length perpendicular to the foam rise direction would be recommended, to compare the strength and modulus with that obtained in the testing already undertaken. This is important because foam (reinforced foam in particular) is known to have highly anisotropic properties.

5.2.9 Fatigue Testing

Time and resources did not allow for fatigue testing, although this could be beneficial due to the product possibly receiving cyclic loads and impacts.

5.2.10 Testing of Foam Produced with Manufacturing Methods

The mechanical mixing used for laboratory foam preparation would likely not be used for production, as impingement mixing of foam components is more common industrially. Therefore, repeating some or all of the tests undertaken in this research project may be beneficial, to examine whether the mixing type affects the properties of the foam or (composite foam).

5.3 Concepts for Future Equipment and/or Techniques

Throughout this research project, it became apparent that benefit could be had if certain technologies were available which have not been conceived yet or the technologies that are available are not suitable to the specific requirements of the products being developed. The most project-relevant concepts are given below, with brief descriptions of the ideas and their purposes. Further development of these concepts is outside the scope of this research project, and may be undertaken by the company for which this research project was undertaken for.

5.3.1 Concept for Internally Plasma Treating Rotomoulded Products

Fibres, films, and other polymer products receive surface treated to increase their ability to be printed or bonded to, but treatment of the inner surface of rotomoulded products is considerably more difficult due the closed, hollow nature of the artefacts made by this moulding process. All the plasma treatment machines found that are currently on the market are designed for treating exterior surfaces, not interior surfaces), such as the equipment shown in Figure 1.20.

Plasma gas cannot be transported, it must be generated within a electromagnetic field, so to treat the inside surface of a rotomoulded product, the product itself will need to become the ‘chamber’, and (for example) an radio frequency (RF) coil wound around it to create a plasma inside the part. This would require complete

sealing of the rotomoulded product and provision for some form of temporary fitting to allow delivery of process gases and a vacuum to be applied to the inner of the product. This could be as simple as drilling and tapping a small hole in one side of the product (a hole will be required anyway for foam filling, so the same hole would be used for both procedures). It is envisaged that the equipment described here should work successfully provided the polymer product is sufficiently strong to not collapse under the required vacuum (of less than 1 Torr) for plasma treatment.

5.3.2 Concept for Performance Increase by Steel Grit Inclusion

When particles of steel grit are added to the rotomoulding cycle with the polymer charge, they have been found to migrate to the inner surface of the part and create a rough surface. This can be utilised when combined with filling the hollow core of the part with a rigid structural foam. The grit becomes keyed into both the rotomoulded skin and the foam filling and has been shown to increase the interfacial bonding strength. The benefits of this system are that no extra processing steps are required, no extra processing equipment needs to be developed, and the steel grit is reasonably cheap considering the small weight fractions that are required. There are no obvious disadvantages other than the slight weight increases resultant from the steel grit, although this could possibly be offset by a lower strength (therefore weight) requirement of the foam which fills the part. A full analysis of this concept would need to be undertaken to confirm these theories and corroborate current test results.

Steps:

1. Put small fraction of steel grit in with polymer charge,
2. Steel grit migrates to inner surface of rotomoulded skin,
3. Steel grit becomes imbedded in skin, but with exposed jagged surfaces,
4. Exposed steel grit keys into foam to restrict shearing of the two surfaces.

5.3.3 Concept for Oxidizing the Inner Surface of a Rotomoulded Part

As a simpler alternative to building custom plasma treatment equipment, the inner surface of the rotomoulded part could be treated by purposely inducing what rotomoulders usually strive to prevent, oxidation. It is hypothesised that by evacuating the air from inside the moulding part toward the end of the heating cycle, then allowing a oxygen-enriched air mixture, for the purpose of oxidising the high temperature polymer, but only the surface, as the bulk of the material has already formed on the mould wall and will therefore be unaffected. Also, the evacuation of the air will limit the oxidation of the polymer in the earlier stages of rotomoulding, allowing the bulk of the polymer to degrade slower than usual.